



HAL
open science

Redox-regulation of photorespiration through mitochondrial thioredoxin o1

Ole Reinholdt, Saskia Schwab, Youjun Zhang, Jean-Philippe Reichheld,
Alisdair Fernie, Martin Hagemann, Stefan Timm

► **To cite this version:**

Ole Reinholdt, Saskia Schwab, Youjun Zhang, Jean-Philippe Reichheld, Alisdair Fernie, et al.. Redox-regulation of photorespiration through mitochondrial thioredoxin o1. *Plant Physiology*, 2019, 181 (2), pp.442-457. 10.1104/pp.19.00559 . hal-02290017

HAL Id: hal-02290017

<https://univ-perp.hal.science/hal-02290017>

Submitted on 27 Jan 2020

HAL is a multi-disciplinary open access archive for the deposit and dissemination of scientific research documents, whether they are published or not. The documents may come from teaching and research institutions in France or abroad, or from public or private research centers.

L'archive ouverte pluridisciplinaire **HAL**, est destinée au dépôt et à la diffusion de documents scientifiques de niveau recherche, publiés ou non, émanant des établissements d'enseignement et de recherche français ou étrangers, des laboratoires publics ou privés.

1Redox-regulation of photorespiration through mitochondrial thioredoxin o1

2Ole Reinholdt^{1§}, Saskia Schwab¹, Youjun Zhang^{2,3}, Jean-Philippe Reichheld^{4,5}, Alisdair R.
3Fernie^{2,3}, Martin Hagemann¹, and Stefan Timm^{1*}

4

5¹University of Rostock, Plant Physiology Department, Albert-Einstein-Straße 3, D-18059
6Rostock, Germany

7²Max Planck Institute of Molecular Plant Physiology, Am Mühlenberg 1, D-14476 Golm,
8Germany

9³Center of Plant System Biology and Biotechnology, 4000 Plovdiv, Bulgaria

10

11⁴Laboratoire Génome et Développement des Plantes, CNRS, F-66860 Perpignan, France;

12⁵Laboratoire Génome et Développement des Plantes, Université Perpignan Via Domitia, F-
1366860 Perpignan, France

14

15*Correspondence to stefan.timm@uni-rostock.de

16 +49 381 498 6115 (fon) -6112 (fax)

17[§]Footnotes

18Present address of O.R.: Miltenyi Biotec GmbH, Robert-Koch-Straße 1, 17166 Teterow,
19Germany.

20

21Abstract

22Photorespiration sustains photosynthesis in the presence of oxygen due to rapid metabolization
23of 2-phosphoglycolate (2-PG), the major side-product of the oxygenase activity of Rubisco. This
24metabolic intermediate has additionally been shown to directly impede carbon assimilation and
25allocation. Despite the fact that both, the biochemical reactions and the underlying genetics are
26well characterized, information concerning the regulatory mechanisms which adjust
27photorespiratory flux is rare. Here, we studied the impact that the mitochondrial localized
28thioredoxin o1 (TRXo1) has on photorespiratory metabolism. The characterization of a T-DNA
29insertional line (*trxo1*) revealed an increase in the stoichiometry of photorespiratory CO₂ release
30and impaired glycine-to-serine turnover after a shift from high-to-low CO₂, without changes in
31glycine decarboxylase (GDC) expression. These effects were distinctly pronounced in a double
32mutant, where the *TRXo1* mutation was combined with strongly reduced GDC T-protein
33expression. The double mutant (*TxGT*) showed reduced growth in air, but not in high CO₂,
34decreased photosynthesis and accumulated up to 54-fold more glycine alongside several redox-
35stress-related metabolites. Given that GDC proteins are potential targets for redox-regulation,
36we also examined the *in vitro* properties of recombinant GDC L-proteins (LPD) from plants and
37the cyanobacterium *Synechocystis* and observed a redox-dependent inhibition by either artificial
38reducing agents or TRXo1 itself. Collectively, our results demonstrate that TRXo1 potentially
39adjusts photorespiration via redox-regulation of GDC in response to environmental changes.

40Introduction

41Photorespiration is an essential process in all organisms performing oxygenic photosynthesis,
42because it is intrinsically linked to photosynthetic CO₂ fixation via Rubisco that catalyzes the
43carboxylation but also oxygenation reaction (Bauwe et al., 2012; Appel et al., 2013). During
44carboxylation, CO₂ is incorporated into the acceptor ribulose-1,5-bisphosphate (RuBP) leading to
45the formation of two 3-phosphoglycerate (3-PGA) molecules that enter the Calvin-Benson cycle
46(CBC). In the Rubisco oxygenase reaction RuBP can also accept O₂ yielding one 3PGA and one
472-phosphoglycolate (2-PG) molecule (Bowes et al., 1971). 2-PG is a non-CBC intermediate that
48is exclusively metabolized by the photorespiratory C2 cycle (Somerville and Ogren, 1979). In
49addition to the main function of photorespiration as organic carbon salvage pathway, efficient 2-
50PG degradation is essential for plant metabolism, because 2-PG acts as a potent inhibitor of
51many enzymes in the chloroplastial stroma, such as triose-phosphate isomerase,
52phosphofructokinase and sedoheptulose-1,7-bisphosphate phosphatase (Anderson, 1971; Kelly

53and Latzkow, 1976; Flügel et al., 2017; Levey et al., 2019; Li et al., 2019). Hence, 2-PG
54accumulation significantly reduces the efficiency of CO₂ assimilation through impairment of the
55CBC and starch biosynthesis.

56Following the early discovery of the light-induced photorespiratory gas-exchange (Zelitch, 1964;
57Tolbert, 1971; Ogren and Bowes, 1976), a broad range of photorespiratory mutants of the C3
58plants *Arabidopsis*, barley, pea, and tobacco, were generated to facilitate the molecular analysis
59of this important process. These mutants showed the characteristic photorespiratory phenotype,
60i.e. they could not grow at ambient air conditions but could be rescued in the presence of
61enhanced CO₂ supplementation (e.g. summarized in: Blackwell et al., 1988; Leegood et al.,
621995; Somerville, 2001; Timm and Bauwe, 2013). More recently, photorespiratory mutants of
63organisms performing a carbon concentrating mechanism such as cyanobacteria, red and green
64algae (Suzuki et al., 1989; Nakamura et al., 2005; Eisenhut et al., 2008; Rademacher et al.,
652016) as well as C4 plant species (Zelitch et al., 2009; Levey et al., 2019) were obtained, which
66also showed the photorespiratory phenotype, supporting the view of photorespiration as
67essential partner of photosynthesis in oxygen-rich atmospheres. The detailed physiological and
68molecular characterization of all these mutants has generated a comprehensive picture of
69photorespiration, including the biochemical pathway, the underlying genetics and how
70photorespiration is embedded in the network of primary metabolism and interacts with many
71other pathways within the entire cellular context (e.g. reviewed in: Wingler et al., 2000; Reumann
72and Weber, 2006; Foyer et al., 2009; Bauwe et al., 2010; 2012; Fernie et al., 2013; Hodges et
73al., 2016; Obata et al., 2016; Timm et al., 2016).

74In contrast to our broad knowledge on function of photorespiration, less progress has been
75made with regards to potential regulatory mechanisms within the photorespiratory cycle. Existing
76data indicate that the mitochondrial glycine-to-serine interconversion, catalyzed through glycine-
77decarboxylase (GDC) in conjunction with serine-hydroxymethyltransferase (SHMT1), potentially
78represent target sites for the regulation of photorespiration. The importance of the GDC and
79SHMT reactions are based on three facts. First, during glycine-to-serine conversion, CO₂ and
80ammonia are liberated. Hence, this step of photorespiration emerged as the prime target for
81genetic engineering approaches to increase crop productivity (Peterhänsel et al., 2013; Betti et
82al., 2016; Walker et al., 2016; South et al., 2018). Secondly, GDC activity was found to be a key
83component in the control of photosynthesis and plant growth (Timm et al., 2012; 2015; 2016;
84Simkin et al., 2017; López-Calcano et al., 2018). Thirdly, the GDC reaction cycle requires four
85cooperating proteins GDC-P, GDC-T, GDC-H and GDC-L, where the latter is also involved in the

86reaction cycle of other enzymatic complexes, which indicates that this biochemical activity needs
87proper regulation (Douce et al., 2001; Timm et al., 2015).

88It has been already shown that, in addition to light-induced transcriptional and translational
89activation of GDC (Walker and Oliver, 1986; Vauclare et al., 1996; Timm et al., 2013), the GDC
90activity in plant mitochondria appears to be sensitive to redox changes. Especially, the NADH
91and NAD⁺ levels are of importance, thereby an increased NADH/NAD⁺ ratio strongly impedes
92glycine-to-serine turnover (Bourguignon et al., 1988). Isolated GDC could be also competitively
93inhibited by serine ($K_i \sim 4$ mM) (Oliver and Sarojini, 1987). Finally, GDC activity can be also
94modulated via post-translational modification. For example, Palmieri et al (2010) showed
95regulation of GDC activity by S-nitrosylation and S-glutathionylation of GDC-H and GDC-P,
96respectively. Moreover, Hodges et al. (2013) reported phosphorylation of several GDC proteins
97and proposed that those modifications might contribute to activity regulation. Proteomic analyses
98provided evidence that all four GDC proteins contain conserved cysteine residues and therefore
99might undergo redox-regulation *in vivo* (Balmer et al., 2004; Keech et al., 2017; Pérez-Pérez et
100al., 2017). Indeed, it was demonstrated that recombinant cyanobacterial GDC P-protein could be
101activated under reducing conditions (Hasse et al., 2013).

102The above-mentioned results make it likely that the glycine-to-serine interconversion is
103modulated via redox-regulation at multiple points. Hence, we investigated whether a
104mitochondrial thioredoxin (TRXo1) is involved in the potential redox regulation of
105photorespiratory reactions in this compartment. To this end, we compared the photosynthetic
106gas-exchange and the metabolic acclimation toward altered CO₂ partial pressure and light
107conditions of the T-DNA insertional line *trxo1* (*trxo1-1*; Daloso et al., 2015) and a newly
108generated double mutant (*TxGT*), which is defective in *TRXo1* expression and strongly reduced
109in the GDC T-protein (*gldt1-1*; Timm et al., 2018). Moreover, we performed *in vitro* LPD activity
110measurements using isolated mitochondria or recombinant proteins to provide direct
111experimental evidence for redox-regulation of GDC. Collectively, our results provide evidence
112that TRXo1 is involved in the regulation of mitochondrial photorespiration and thus contributes to
113the adaptation of the photorespiratory flux towards changes in the environmental conditions that
114affect the subcellular redox-state.

115Results

116Deletion of *TRXo1* causes an increase in the stoichiometry of photorespiratory CO₂ 117release

118In general, mutants defective in photorespiration or associated processes exhibit a distinct
119negative impact on the photosynthetic gas exchange (e.g. Dellero et al., 2015; Eisenhut et al.,
1202013a; Pick et al., 2013; Timm et al., 2012). Apart from constraints within the core cycle, deletion
121of genes that encode for proteins of accessory functions were characterized by an increase in
122the stoichiometry of photorespiratory CO₂ release, particularly under conditions that require
123photorespiration to operate at high efficiencies (Cousins et al., 2011; Timm et al., 2011). To test
124whether *TRXo1* mutation impacts photorespiratory metabolism, the T-DNA insertional line *trxo1*
125(*trxo1-1*; Daloso et al., 2015) and the wild type were subjected to varying oxygen concentrations
126(3, 21, 40, and 50% O₂) during gas exchange measurements. As shown in Fig. 1A, *trxo1*
127showed no alteration in the net CO₂ assimilation rate (A) at low or normal photorespiratory flux (3
128and 21% O₂), which is in agreement with unaltered growth in normal air (Daloso et al., 2015), but
129significant decreased photosynthesis at enhanced O₂ concentrations (40 and 50%) that
130stimulate a higher flux through photorespiration. Hence, O₂ inhibition of A (Fig. 1B) was
131significantly higher in *trxo1* (47.7 ± 4.0%) compared to the wild type (38.3 ± 4.1%). In
132accordance with the decrease in A, the CO₂ compensation point (Γ) is unchanged at 3 and 21%
133O₂ but significantly higher in *trxo1* at 40 and 50% O₂ (Fig. 1C). These changes increase the
134slope (γ) from the estimated Γ-versus-oxygen response lines to about 20% (Fig. 1D), indicating a
135higher fraction of CO₂ released from photorespiration.

136Metabolic effects of *TRXo1* deficiency on glycine turnover and cellular redox components

137To further substantiate whether mitochondrial localized TRXo1 (Daloso et al., 2015) contributes
138to mitochondrial photorespiration we next performed metabolomics during CO₂ transition using
139liquid chromatography coupled to tandem mass spectrometry (LC-MS/MS). Rationally, CO₂
140concentrations were varied to distinguish between states with suppressed photorespiration (high
141CO₂, HC, 1500 ppm) and two stages with active photorespiration that are 1 and 9 h after transfer
142of the plants into normal air (390 ppm). For comparison, we included the GDC T-protein
143knockdown mutant *gldt1*, characterized by a ~70% reduction in total GDC activity (*gldt1-1*; Timm
144et al., 2018). In agreement with previous studies (Timm et al., 2012; Eisenhut et al., 2016), the
145glycine content of wild type increased (~3.8 fold) 9 h after the transfer into normal air (Fig. 2)

146(Timm et al., 2012; Eisenhut et al., 2016). However, a distinct, intermitted glycine accumulation
147(~38 fold) was visible after 1 h in normal air. This accumulation kinetics was most pronounced
148but not restricted to glycine, since other photorespiratory intermediates such as glyoxylate, 3-
149hydroxypyruvate (3HP), glycerate, and 3-PGA followed a similar trend (Fig. 2). Interestingly, the
150redox-related compounds glutathione (GSH), cysteine and cystine also followed the pattern of
151the photorespiratory intermediates. Serine, as the product of GDC/SHMT reactions, behaves
152almost inverse to the changes observed in glycine. The wild type shows a transient drop in
153serine after 1 h in normal air but its absolute amount returned to HC levels after 9 h in normal air
154(Fig. 2). Compared to wild type, the transient glycine accumulation in *trxo1* is much lesser
155pronounced (~ 4.2 fold), but its content is considerably higher (~43 fold) after 9 h in normal air
156(Fig. 2). The missing intermitted increase was also observed in the other photorespiratory
157intermediates, which were all lower after 1 h in normal air or invariant (glyoxylate, 3HP and
158glycerate) compared to the wild type after 9 h in normal air. Only 3-PGA, the primary
159carboxylation product of Rubisco, was significantly decreased in *trxo1* after 9 h in normal air
160(Fig. 2). No intermitted accumulation was also seen in the three redox components after 1 h
161whilst higher levels of GSH and cysteine were observed after 9 h in normal air in *trxo1*. As
162expected, reduction of GDC activity to ~30% impairs glycine-to-serine interconversion in *gldt1*
163and thus causes a nearly linear increase in glycine up to 71-fold after 9 h LC compared to HC, a
164trend that was also reflected in GSH, cysteine and cystine levels. Concerning the other
165photorespiratory intermediates, an increase in the upstream intermediate glyoxylate after 9 h in
166normal air was found. The downstream metabolites 3HP and glycerate were significantly
167decreased only after 1 h and invariant after 9 h in normal air. Only 3-PGA was lower in *gldt1* in
168these two time points (Fig. 2). Other than the wild type, *trxo1* and *gldt1* showed a continuous
169decrease in the GDC/SHMT reaction product serine after the shift into normal air. Unsurprisingly,
170these changes sum up to a gradually increasing glycine-to-serine ratio in both mutants, whereas
171the increase in the wild type is only on a short-term (Fig. 2). From these results one can
172conclude that the most dominant effect is related to metabolites of GDC operation and redox
173regulation in both mutants.

174Apart from changes in intermediates related to photorespiration and redox buffering, deletion of
175*TRXo1* also affected metabolite levels from the TCA-cycle. While several pathway intermediates
176(e.g. malate, citrate, fumarate and aconitate) show short-term accumulation followed by
177normalization or a steadily increase (succinate) in the wild type, they did not transiently increase
178and did not show major fluctuations during CO₂ transition in *trxo1* (Fig. 2; Supp. Table 1). A
179similar behavior was observed in *gldt1*, with the exception of an approximately 4-fold

180accumulation of succinate. Finally, *gldt1* accumulates branched chain (valine, isoleucine and
181leucine) and aromatic (phenylalanine, tryptophan and tyrosine) amino acids upon the transfer
182into normal air as previously reported for other photorespiration mutants (Timm et al., 2012;
183Eisenhut et al., 2017; Orf et al., 2016). Again, *trxo1* behaved differently, since it showed only
184minor variations in the branched chain and aromatic amino acid contents after 9 h, but lacked
185the intermittent increases in the branched chain, but not aromatic amino acids, after 1 h in
186normal air as observed for wild type leaves (Fig. 2; Supp. Table S1).

187**Lack of *TRXo1* does not affect mRNA expression and protein abundance of** 188**photorespiratory genes/proteins**

189Given that the altered glycine-to-serine interconversion in *trxo1* could be due to an altered
190expression of the enzymes participating in photorespiration, we next analyzed mRNA and
191protein contents of enzymes involved in the mitochondrial steps of photorespiration. To this end,
192leaf-material of *trxo1* and the wild type was harvested at the end of the day (9 h illumination) in
193normal air and qRT-PCR and immuno-blotting experiments were carried out. As shown in Fig. 3,
194we never observed significant alterations in neither mRNA nor protein levels of all four GDC
195genes and the major photorespiratory SHMT1 isoform. Similarly, constant expression was also
196detected in all three genes that served as controls for photorespiratory enzymes not localized in
197the mitochondrion (Fig. 3), namely peroxisomal hydroxypyruvate reductase 1 (HPR1),
198peroxisomal malate dehydrogenase (pMDH) and chloroplastic 2-PG phosphatase (PGLP).

199**Deletion of *TRXo1* in the *gldt1* background intensifies the photorespiratory phenotype**

200Next we hypothesized that if *TRXo1* affects GDC activity, phenotypic and physiological
201alterations would be exacerbated in mutants that exhibit combined defects in *TRXo1* and *GDC*
202expression under photorespiratory conditions. For this reason, *trxo1* was crossed with the *gldt1*
203knock-down mutant (5% residual *GDC-T* mRNA expression; Timm et al., 2018) to obtain the
204double mutant *TxGT* (for genotypic verification see Supp. Fig. S1). As shown in Fig. 4A, wild
205type and *trxo1* plants grew similarly (unchanged rosette diameter and leaf number) and were
206invariant from each other with regard to chlorophyll a fluorescence. In agreement with previous
207findings (Timm et al., 2018), *gldt1* showed reduced growth (reduction in the rosette diameter),
208yellowish leaves, and lowered F_v/F_m under photorespiratory conditions. Interestingly, the
209reduction of growth and PSII efficiency observed in the *gldt1* mutant was further enhanced in the
210*TxGT* line (Fig. 4A). The slower growth of *gldt1* and *TxGT* mutant lines also caused delayed
211onset of flowering for approximately one and three weeks, respectively. If plants were cultivated

212in HC, suppressing photorespiration, growth of the *gldt1* and *TxGT* lines are fully restored to wild
213type levels as reflected by the unchanged rosette diameter and total leaf number, while *TxGT*
214still showed a significant decrease in F_v/F_m (Fig. 4B). Collectively, CO₂ dependent
215complementation of growth suggests that the stronger phenotypic alterations in *TxGT* are due to
216an additive, negative impact on photorespiration.

217**Mutation of *TRXo1* and *GDC-T* does not affect expression of photorespiratory proteins**

218To exclude that the intensified signs of the photorespiratory phenotype are due to altered
219expression of photorespiratory enzymes in the double mutant, we carried out immunoblot
220analysis from all mutants in comparison with the wild type in a CO₂ transfer experiment as done
221for metabolite profiling before. To this end, leaf material was harvested from 8 week old plants in
222HC (9 h light) and normal air (1 and 9 h light, respectively) and compared to each other.
223Expression analysis was restricted to the protein level, since mRNA levels of photorespiratory
224genes were found to be unaffected during CO₂ transition (Eisenhut et al., 2016). With regards to
225mitochondrial photorespiration, we did not observe any major and systematic change in the
226expression of GDC proteins (P, L and H) or SHMT1 (Supp. Fig. S2). Furthermore, other
227photorespiratory proteins (PGLP and HPR1) as well as RbcL, the E2 subunits of the
228oxoglutarate dehydrogenase complex (OGDC) and the pyruvate dehydrogenase complex
229(PDHC) from the TCA-cycle did also not change in all genotypes at different CO₂ conditions
230(Supp. Fig. S2). Thus, this experiment demonstrates that neither the knock down of *GDC-T* or
231the knockout of *TRXo1* alone nor the combination of both alter the abundance of
232photorespiratory core enzymes during CO₂ transition.

233**The double mutant *TxGT* exhibits strong impairment of photosynthetic CO₂ assimilation**

234Given the distinct phenotype of the *TxGT* double mutant, its photosynthetic capacity was next
235characterized in more detail. Due to the smaller leaves of air-grown *TxGT*, which prevents
236appropriate gas-exchange measurements, plants were first grown in HC for 7 weeks to
237synchronize growth. After transfer to normal air and acclimation for 1 week, *gldt1*, *TxGT* and
238wild-type plants were analyzed. As depicted in Fig. 5, values of A, Γ , oxygen inhibition and γ in
239wild-type plants are similar to plants consequently grown in normal air (see Fig. 2). However, the
240*gldt1* mutation has a negative impact on CO₂ assimilation, which steadily increased during
241measurements with elevated O₂ concentrations. Accordingly, A and Γ of *gldt1* are reduced by
242about 18% and 14% at low O₂ (3%) but by about 58% and 35% in a high O₂ (50%) atmosphere,
243respectively (Fig. 5A and C). These changes summed up to an ~80% increase in O₂ inhibition of
244A and ~116% of γ (Fig. B and C). These alterations are elevated in the *TxGT* plants grown for

245one week in normal air. Hence, the decreases in A (~37%) and Γ (~57%) are already larger at
246low O₂ and significantly higher at 50% O₂ (A - ~83%; Γ - ~86%) (Fig. 5A and C). These inhibitory
247effects also resulted in increased O₂ inhibition of A (~117%) and enhanced γ (~85%) (Fig. 5B
248and D). Collectively, these data suggest an additive, negative impact of both mutations on
249photorespiration, and in turn, photosynthesis.

250Impairment of mitochondrial photorespiration alters pyridine nucleotide contents

251The above mentioned results provided evidence that *TRXo1* deficiency impacts mitochondrial
252photorespiration, particularly GDC, known to be the major source of NADH production in
253illuminated leaves (Leegood et al., 1995). Moreover, *TRXo1* belongs to the cellular TRX system
254which is directly linked to the cellular pyridine nucleotide pools, because NADPH-dependent
255thioredoxin reductases (NTR) use NADPH as reducing power for various TRX proteins
256(Geigenberger et al., 2017). Consequently, we next quantified the abundances of pyridine
257nucleotides (NAD⁺, NADH, NADP⁺ and NADPH) in all genotypes during CO₂ transition. In HC,
258we did not observe significant alterations in NAD⁺, NADH and the NADH/NAD⁺ ratio between
259these genotypes (Fig. 6A, B and C), except a slight increase in the NADH/NAD⁺ ratio in the
260*TxGT* mutant (Fig. 6C). After the transfer to normal air for 1 h, all genotypes display decreased
261NADH and higher NAD⁺ abundances (except *gldt1*), leading to significant reductions in the
262NADH/NAD⁺ ratio in all mutants if compared to the wild type (Fig. 6A, B and C). These changes
263mostly disappeared after 9 h in normal air, but all mutants consistently showed slightly
264decreased NADH amounts compared to wild type (Fig. 6A, B and C). Comparable changes were
265observed in the amounts of the phosphorylated pyridine nucleotide abundances. In HC, only the
266*TxGT* mutant elevated NADPH and decreased NADP⁺ levels, while the NADPH/NADP⁺ ratio is
267higher in the *trxo1* and *TxGT* lines (Fig. 6D, E and F). After the transfer to normal air for 1 as well
268as 9 h, NADPH is significantly decreased in all genotypes (Fig. 6D), whereas NADP⁺ is only
269transiently elevated in *trxo1* and *TxGT* (Fig. 6E). However, all mutant lines are characterized by
270a significant decrease in the NADPH/NADP⁺ ratio at both time points in air (Fig. 6F).

271The double mutant *TxGT* shows the characteristic photorespiratory metabolic signature

272Next we analyzed how the combined mutation of *TRXo1* and *GDC-T* affects the steady-state
273metabolite profile in *TxGT*. To this end, leaf material from plants grown in either HC (1500 ppm
274CO₂) or normal air (390 ppm CO₂) was harvested after 9 h of illumination under both conditions
275and selected metabolites were quantified by LC-MS/MS analysis. As shown in Fig. 7, glycine
276was invariant between the wild type and *trxo1* in HC, but it already increased in *gldt1* (~1.7-fold)
277and *TxGT* (~3.5-fold) under this condition. In normal air, leaves of the wild type and the *trxo1*

278mutant contain similar amounts of glycine compared to HC. However, a much stronger increase
279in glycine was observed in leaves of *gldt1* (~17-fold) and especially *TxGT* (~54-fold) under
280ambient air conditions. These changes, together with the largely unaltered serine amounts in all
281plant lines, caused also a significant elevation of the cellular glycine-to-serine ratio. Only in *gldt1*
282and *TxGT* it was already higher at HC (~1.7- and ~2.5-fold) and increased further in normal air
283(~13.8- and ~43.5-fold) conditions.

284Other photorespiratory intermediates did not significantly change between the genotypes after
285growth in HC, except a slight increase in 3HP in the *TxGT* mutant. Under ambient air conditions,
286however, we found elevated amounts of glyoxylate (significant in *gldt1* and *TxGT*) and
287decreased amounts of glycerate (all lines) and 3-PGA (significant in *trxo1* and *TxGT*) in the
288mutants compared to the wild type (Fig. 7). Only 3HP did not follow this trend given its content
289was slightly higher in *trxo1* and *TxGT*. The compounds related to redox-homeostasis were also
290analyzed in this experiment and compared to the results shown in Fig. 2. Except a slight
291increase in GSH and cysteine in *TxGT*, all three compounds were basically unaltered between
292the other genotypes and the wild type under HC conditions (Fig. 7). Growth in normal air
293significantly changed the amounts of all three intermediates. In the wild type, GSH, cysteine and
294cystine are lower compared to HC (Fig. 7). In the mutants, however, all three intermediates
295showed gradually increased amounts in the order of their negative impact on photorespiration
296(*trxo1* < *gldt1* < *TxGT*).

297Apart from these changes, several other metabolic alterations previously observed in *trxo1* (Fig.
2982, Supp. Table S1) and *gldt1* (Timm et al., 2018) are much more pronounced in the *TxGT* double
299mutant (Supp. Table S2). For example, *TxGT* accumulates higher amounts of the branched
300chain amino acids valine (~2.7-fold), isoleucine (~4.2-fold) and leucine (~9.1-fold) as well as the
301aromatic amino acids phenylalanine (~4.2-fold), tryptophan (~5.5-fold), and tyrosine (~6.6-fold)
302in normal air compared to the wild type (Fig. 7; Supp. Table 2). Enhanced accumulation was
303also seen for proline, histidine, arginine, and asparagine, while alanine and aspartate were
304strongly decreased in *TxGT*. Finally, changes were also observed in the amounts of some TCA-
305cycle intermediates. For example, malate (~2.0-fold) and citrate (~3.6-fold) were elevated while
306fumarate (~16% of the wild type) was decreased (Fig. 7; Supp. Table S2). In summary, the
307combined mutation of *Trxo1* and *GDC-T* enhances the negative impact on GDC activity and
308causes a metabolic signature comparable to that observed with other mutants showing a strong
309photorespiratory phenotype (Timm et al., 2012; Eisenhut et al., 2016; Orf et al., 2016; Levey et
310al., 2018).

311 Redox-regulation of the GDC L-protein from pea and *Synechocystis* through TRXo1

312 Given that the GDC expression is unchanged in *trxo1* and the *TxGT* double mutant (see Fig. 2,
313 Supp. Fig. S2), only alterations in the GDC activity could account for the altered glycine
314 accumulation in the mutants. Since H-protein is not enzymatically active and we also observed
315 stronger negative impact on GDC performance in the double mutant with very low GDC-T
316 amounts, we next tested if the GDC-L protein (LPD) activity can be redox-regulated. For this
317 purpose, activity measurements were carried out using LPD from three different sources, namely
318 isolated *Pisum sativum* (pea) leaf-mitochondria (native mtLPD), recombinant mtLPD from pea
319 (*Psm*tLPD), and recombinant LPD from the cyanobacterium *Synechocystis* PCC 6803 (SyLPD)
320 produced and purified after heterologous expression in *E. coli*. As a representative from a non-
321 photosynthetic organism we further included LPD from *E. coli* for comparison. As shown in Fig.
322 8, LPD activity from the phototrophic hosts is clearly inhibited upon addition of the artificial
323 reducing agent dithiothreitol (DTT). Its activity decreased to about ~43% (native mtLPD, Fig.
324 8A), ~52% (*Psm*tLPD, Fig. 8B) and ~15% (SyLPD, Fig. 8C). Such inhibitory effects were not
325 observed during measurements with *E. coli* LPD (Fig. 8D). Reduction in LPD activity (~35%,
326 ~31% and ~32% for native mtLPD, *Psm*tLPD and syLPD, respectively) from photosynthetic
327 organisms is also caused through addition of the natural reductant TRXo1 in combination with
328 the NADPH-dependent thioredoxin reductase a (NTRa). Notably, the observed inhibition is due
329 to the activity of the TRXo1/NTRa redox-couple, since no alterations in LPD activity were
330 observed with inactive TRXo1/NTRa (Fig. 8). In summary, these experiments provide evidence
331 that LPD of the plant and cyanobacterial GDC, but not from a heterotrophic organism such as *E.*
332 *coli*, undergoes redox-regulation.

333 Finally, to pinpoint critical amino acid residues in the LPD proteins used during this study (pea,
334 *Synechocystis* and *E. coli*) we analyzed the respective protein sequences in more detail and in
335 comparison to other plant (*Arabidopsis*, maize) and bacterial (*Azotobacter vinelandii*,
336 *Pseudomonas putida*) representatives. Rationally, the presence of conserved cysteine residues
337 could help to explain a functional mechanism that might involve disulfide bond formation through
338 TRX proteins, presumably TRXo1, in the LPD proteins used during this study (pea,
339 *Synechocystis* and *E. coli*). All of the analyzed LPD sequences contain two conserved cysteine
340 residues (Cys 45 and Cys 50; Supp. Fig. S3). Previous work has suggested that these residues
341 form a disulfide bond that is involved in FAD-binding and might be of importance for the
342 interaction with the GDC-H protein (Faure et al., 2000). Interestingly, we also found cysteine
343 residues (Cys 34, Cys 335 and Cys 446) that are conserved only in LPD proteins from higher

344plants and also in *Synechocystis* (Cys 34 and Cys 335), but apparently are absent in the
345proteins from heterotrophic organisms (Supp. Fig. S3). Based on the existing crystal structure of
346the pea LPD protein (Faure et al., 2000), we generated *in silico* models of the pea,
347*Synechocystis* and *E. coli* LPD proteins (Supp. Fig. 4) to find out whether Cys 34, Cys 335 and
348Cys 446 are in close vicinity in the 3D structure and thus allow disulfide bond formation that
349could potentially be involved in the redox-regulation of LPDs from photosynthetic organisms.
350Indeed, all three Cys residues are relatively close to each other between the FAD-binding (Cys
35134), the central (Cys 335) and the interface domain (Cys 446). Given that Cys 446 is not present
352in *Synechocystis* (redox-regulated), but present in *E. coli* (not redox-regulated), it seems unlikely
353that this residue is important for activity regulation. Therefore, we conclude that a TRX could
354potentially form or split a disulfide bond between Cys 34 and Cys 335 to redox-regulate LPD
355activity.

356Discussion

357Photorespiration has attracted major interest in plant research and is the currently one of the
358major targets in plant breeding (Peterhänsel et al., 2013; Betti et al., 2016; Walker et al., 2016;
359South et al., 2018; 2019). However, regulatory aspects of photorespiration have been only
360scarcely investigated. To date, no protein with regulatory impact on photorespiration was
361identified either via classic randomized mutation screens (Somerville, 2001; Badger et al., 2009)
362or other procedures (Carroll et al., 2015). The failure to identify regulatory candidates by these
363strategies could be explained by the fact that regulatory mutants might display a rather weak
364photorespiratory phenotype or that those proteins are often encoded by redundant gene families
365(Somerville, 2001; Timm and Bauwe, 2013). Nevertheless, there are several hints that some
366photorespiratory steps such as GDC in the mitochondrion might be prone to redox regulation
367(Balmer et al., 2004; Keech et al., 2017; Pérez-Pérez et al., 2017). Accordingly, we used a T-
368DNA insertional mutant that lacks the mitochondrial *TRXo1* (Daloso et al., 2015) to analyze its
369potential contribution to redox regulation of photorespiration.

370*TRXo1* contributes to photorespiratory metabolism

371The *trxo1* single mutant provides some evidence that this protein could indeed be involved in
372redox regulation of photorespiration. As such it is perhaps unsurprising that, it shows an
373increase in the stoichiometry of photorespiratory CO₂ release, which was previously observed
374also in other mutants with a moderately, constrained photorespiratory flux (Cousins et al., 2011;
375Timm et al., 2011). Further support that *TRXo1* impacts mitochondrial photorespiration was

376 provided from our metabolite analysis (Fig. 2). Whilst rather minor changes in the glycine-to-
377 serine conversion were observed if *trxo1* was consequently grown in normal air (Fig. 7; Daloso
378 et al., 2015), clear differences in glycine accumulation were found if the mutant was shifted from
379 HC into air to simulate quick photorespiratory activation (Fig. 2). Hence, TRXo1 mediated
380 regulation could play a more dominant role in the short term acclimation of photorespiration to
381 fluctuating environments. In wild-type leaf material, glycine is low under HC conditions but
382 increased about 38-fold after 1 h in LC before it returned to only slightly enhanced levels (~3.8
383 fold) after 9 h. This strong transient glycine accumulation shortly after induction of
384 photorespiration is consistent with previous reports (Timm et al., 2012; Eisenhut et al., 2016; Orf
385 et al., 2016) and points to the necessity that glycine turnover via GDC needs some activation
386 after HC to LC shifts. Interestingly, such intermittent strong effects on glycine were not found in
387 *trxo1*, here the glycine level rose somewhat continuously from 1 to 9 h in LC. This finding
388 indicates that TRXo1 mediated redox control could somehow inhibit GDC activity in cells grown
389 at HC, which is relieved in the *trxo1* mutant on a short term and in wild type only after longer
390 acclimation to LC conditions. A likely candidate for the TRXo1-mediated redox regulation of
391 GDC is mtLPD since its activity decreases when reduced via this protein (Fig. 8, discussed
392 below in detail). Transient accumulation of the redox-related intermediates GSH, cysteine and
393 cystine in wild-type leaves (Fig. 2) is consistent with the hypothesis that fast HC to LC shifts
394 might result in a transient redox shift in mitochondria, which is lesser pronounced in the *trxo1*
395 mutant. Notably, short term effects on redox-stress intermediates in the wild type can, at least
396 partially, be related to GDC activation. This can be concluded from studies on the *gldt1* mutant,
397 which exhibits an approximate 70% reduction in the total GDC activity (Timm et al., 2018), since
398 it displays increases in these metabolites similar to the wild type after 1 h in LC, but all
399 intermediates do further increase considerably without optimal GDC activity (Fig. 2).
400 Malfunctioning of GDC reduces NADH regeneration and in turn leads to an undersupply of the
401 respiratory chain. This assumption is supported by our quantification of pyridine nucleotide
402 contents during CO₂ transition, which revealed a higher NADH/NAD⁺ ratio in the wild type (Fig.
403 6) in agreement with a higher photorespiratory flux through GDC and thus, increased NADH
404 production. In contrast, impairment of GDC activation/activity in both, *trxo1* and *gldt1*,
405 respectively, causes a distinct drop in the NADH/NAD⁺ ratio (Fig. 6). As expected, these effects
406 are mostly seen shortly after HC to ambient air transfer and became somewhat alleviated after 9
407 h. However, these results provide clear evidence that proper GDC regulation is crucial to
408 maintain the cellular redox-homeostasis. Imbalances of it, particularly in mitochondria, eventually

409cause higher production of reactive oxygen species (ROS) that might be counteracted via the
410accumulated GSH (Fig. 2).

411However, the observed effects of the single *TRXo1* mutation on photorespiration and related
412metabolites are rather weak under standard conditions. Such a behavior has been predicted for
413other regulatory mutants (Timm and Bauwe, 2013). Moreover, *TRXo1* is not the only
414mitochondrial TRX in Arabidopsis. It is known that *TRXh2* is also present in mitochondria
415(Daloso et al., 2015) and we currently cannot rule out some redundancy between these two
416proteins, thus weakening the phenotype of single *trxo1* mutant. Given the fact that changes in
417the phosphorylated pyridine nucleotide contents during CO₂ transition are most dominant in the
418*trxo1* and *TxGT* mutants shortly after transfer into normal air (Fig. 6D, E and F) it is likely that the
419decrease of the NADPH/NADP⁺ ratio can only be partially referred to the feedback inhibition on
420photosynthesis, particularly the CBC, in response to malfunctioning of photorespiration (Timm et
421al., 2016). The stronger, intermitted responses in mutants lacking *TRXo1* could also lead to
422activation of other TRX proteins that require a higher NADPH turnover through NTRa. Hence,
423*TRXh2* might, at least to some extent, compensate for the loss of *TRXo1* and also act on GDC
424proteins to regulate their activity. Indeed, similar observations have been made with several TRX
425target enzymes of the TCA-cycle (Daloso et al., 2015) and future research on multiple mutants is
426needed to elucidate the interplay between the different TRX proteins and their regulation of
427GDC.

428**Lack of *TRXo1* in a *GDC-T* knock down mutant intensifies the photorespiratory phenotype**

429To further substantiate the impact of *TRXo1* on mitochondrial photorespiratory metabolism, we
430took advantage of a double mutant approach. For this purpose, *trxo1* was crossed into the *gldt1*
431background, to follow how plant metabolism adapts if overall GDC capacity is decreased to
432about 70% (*gldt1*; Timm et al., 2018) and additionally lacks the possible *TRXo1* mediated redox-
433regulation. The double mutant *TxGT* showed a more strongly pronounced photorespiratory
434phenotype than *gldt1*. Growth, PSII activity, and photosynthetic CO₂ assimilation were clearly
435diminished when cultivated in normal air but remained unaltered if grown in HC (Fig. 4, and 5).
436These changes provide strong evidence that the *TRXo1* and *GDC-T* mutations are negatively
437additive for photorespiratory metabolism in mitochondria; i.e. the double mutant *TxGT* clearly
438amplifies the importance of *TRXo1* for photorespiration. This finding could indicate that the
439absence of *TRXo1* further decreases the GDC activity, but not necessarily through affecting the
440cellular redox-state as evident by the observation that changes in the pyridine nucleotide

441 contents are similar between the *trxo1* and the *TxGT* mutant (Fig. 6). In this scenario, activity
442 regulation of GDC could occur directly only on GDC-P or GDC-L, since GDC-H is not
443 enzymatically active and GDC-T already highly diminished. This assumption is underpinned by
444 the massive increases in glycine and glycine-to-serine ratio (Fig. 7), indicating intensified
445 impairment of GDC.

446 The intensified photorespiratory phenotype can potentially also be explained by missing TRXo1-
447 mediated redox regulation of other processes, indirectly affecting the operation of GDC. It has
448 been shown that the *trxo1* mutant exhibits a deregulated TCA cycle (Daloso et al. 2015), which
449 in turn could affect photorespiration due to their physiological interaction (Obata et al., 2016).
450 Changes in TCA cycle intermediates are obvious in the *trxo1* mutant (Supp. Table 1) and are
451 intensified in the case of malate, citrate and fumarate in the *TxGT* double mutant (Supp. Table
452 2). Moreover, the TRXo1-mediated regulation of mtLPD (Fig. 8) is not only relevant for the
453 regulation of GDC activity, because this protein is also part of the PDHC and OGDC involved in
454 the TCA cycle, as well as the branched-chain 2-oxoacid dehydrogenase complex (BCDHC)
455 involved in the degradation of branch chain amino acid (Oliver et al., 1990; Millar et al., 1998;
456 Timm et al., 2015). Hence, one might speculate that the strongly enhanced photorespiratory
457 phenotype of the *TxGT* plants is partially related to the malfunction of mtLPD in these multiple
458 complexes. Indeed, in support of this theory some characteristic changes in the TCA-cycle and
459 branched chain amino acid metabolism are visible in *trxo1* and *TxGT* under both HC and LC
460 (Supp. Tables 1 and 2).

461 The above facts notwithstanding, the phenotypic complementation of *TxGT* by elevated CO₂
462 levels clearly indicates that the main cause of the phenotype is due to a photorespiratory defect.
463 As indicated by the massively elevated glycine amounts this is presumably mediated by an
464 effect on the GDC activity (Fig. 7).

465 **TRXo1 contributes to redox-regulation of GDC through LPD**

466 As mentioned above, all four GDC (P, T, H and L) proteins contain conserved cysteine residues
467 and, thus, were suggested to undergo redox-regulation (Balmer et al., 2004; Keech et al., 2017;
468 Pérez-Pérez et al., 2017). To date, a redox-regulation mechanism was proposed and
469 experimentally verified only for the *Synechocystis* GDC P-protein (Hasse et al., 2013), the actual
470 glycine decarboxylase. It has been also shown that the entire GDC activity became severely
471 inhibited in a more oxidized and ROS producing mitochondrion due to a defect in the ER
472 localized adenylate transporter 1 (*ER-ANT1*) in Arabidopsis and rice (Hoffmann et al., 2013;

473Zhang et al., 2016), which was partly relieved upon DTT addition (Hoffman et al., 2013). These
474findings stimulated us to test GDC-L (mtLPD) for its potential to undergo redox-regulation, which
475could be based on disulfide bond formation that has been *in silico* predicted onto the LPD
476structure (Faure et al., 2000). LPD proteins from phototrophic and heterotrophic organisms
477(Supp. Fig. S3) all possess conserved cys 45 and cys 50 residues that are likely involved in the
478binding of the FAD-cofactor and interaction with GDC-H (Faure et al., 2000). However, there are
479other cys residues that are only conserved in LPD proteins from phototrophic organisms, which
480thus might play a role in TRXo1-based LPD redox-regulation (Supp. Fig. S4). Consistent with
481this assumption we showed that reducing conditions did not affect LPD from *E. coli* but always
482inhibited LPD activity from phototrophic origin, including native LPD from pea leaf-mitochondria
483and recombinant proteins from pea and *Synechocystis* PCC 6803. In addition to DTT, the
484natural redox-couple consisting of the recombinant mitochondrial TRXo1 and NTRa from
485Arabidopsis (Reichheld et al., 2007; Daloso et al., 2015) were also able to decrease activity of
486the plant and cyanobacterial LPD. Redox regulation of LPD has been recently also suggested in
487experiments to characterize the thioredoxome of Chlamydomonas (Pérez-Pérez et al., 2017). As
488mentioned before, such a regulation is anticipated to not only affect GDC but also the other
489mitochondrial enzyme complexes in which LPD is involved in, namely, PDHC, OGDC, as well as
490BCDHC. Notably, all of the analyzed organic acids involved in the TCA-cycle (malate, citrate,
491succinate and fumarate) as well as the branched chain (valine, isoleucine and leucine), but not
492the aromatic (tyrosine, phenylalanine and tryptophane), amino acids essentially show the same
493accumulation pattern in *trxo1* during HC-to-LC transition as glycine does (Fig. 2, Suppl. Table
494S1).

495The fact that we observed a biphasic response of many metabolites in wild type that was mostly
496absent in the *trxo1* mutants indicates that redox-regulation occurs on different time scales and
497might involve other compensatory mechanisms such as through TRXh2. However, our results
498suggest that TRXo1 is part of the regulation cycle of GDC and the other multi-enzyme systems
499LPD is involved in. First, and on a shorter time scale (e.g., 1 h after shift to ambient air in our
500experiment) the presence of TRXo1 (wild-type situation) controls the activation state of LPD and,
501thus, prevents imbalances in mitochondrial metabolism towards a massive carbon influx into
502photorespiration that affects the mitochondrial redox-state mainly via elevation of the
503NADH/NAD⁺ ratio that in turn would inhibit GDC (Taylor et al., 2002). Given the absence of the
504strong intermittent glycine accumulation in *trxo1*, it appears that absence of TRXo1 facilitates
505glycine turnover on the shorter time scale through a more active LPD and, likely, GDC. A similar
506response was also seen for the intermediates metabolized by PDHC, OGDC, and BCDHC.

507Nevertheless, on a longer time scale and also in the *TxGT* double mutant with a “pre-impaired”
508GDC, absence of TRXo1 no longer facilitates LPD activity. We currently hypothesize that under
509these conditions another TRX protein, presumably TRXh2, compensates for the lack of TRXo1
510to prevent from uncontrolled reduction of NAD⁺, as evident from the higher turnover of NADPH in
511the *trxo1* and the *TxGT* mutant (Fig. 6). Collectively, our results indicate that TRXo1 contributes
512to the regulation of mitochondrial multi-enzyme systems, particularly GDC, in response to short-
513term fluctuations caused by environmental changes.

514Material and methods

515Plant material and growth

516*Arabidopsis thaliana* (*Arabidopsis*) ecotype Col.0 was used as wild type reference during this
517study. T-DNA insertional lines *trxo1-1* (SALK 042792) and *gldt1-1* (WiscDSLox 366A11-085) in
518the Col.0 background were obtained from the Nottingham Arabidopsis Stock Centre (Alonso et
519al. 2003; Woody et al. 2007) and homozygous lines produced as described previously (Daloso et
520al., 2015; Timm et al., 2018). After sterilization with chloric acid, seeds were sown on a
521soil/vermiculite mixture (4:1), incubated at 4°C for 2 days to break dormancy and plants grown
522under controlled environmental conditions as follows: 10 h day, 20°C/ 14 h night, 18°C, ~ 120
523μmol photons m⁻² s⁻¹ light intensity, and 70% relative humidity. Where specified in the text, CO₂
524concentration was increased from 390 ppm (normal air) to 1500 ppm (HC - high carbon) with
525otherwise equal conditions. Plants were regularly watered and fertilized weekly (0.2% Wuxal,
526Aglukon).

527Generation and verification of the *TRXo1* and *GLD-T* double mutant (*TxGT*)

528The *trxo1-1* and *gldt1-1* T-DNA insertional lines were crossed to obtain a *trxo1-1-gldt1-1* double
529mutant (*TxGT*). To verify the T-DNA insertions in both genes in the following generations, leaf
530DNA was isolated according to standard protocols and PCR-amplified (min at 94°C, 1 min at
53158°C, 2 min at 72°C; 35 cycles) with primers specific for the left border (R497 for WiscDsLox
532line, *gldt1-1* or T5 for SALK 042792 line, *trxo1-1*) and *AtGDC-T* (R490) and *TRXo1* (T4) specific
533primers. The resulting fragments (*gldt1-1* 1859 bp, *trxo1-1* 2000 bp) were sequenced for
534verification of the T-DNA fragment within both genes. Zygosity was examined by PCR
535amplification (min at 94°C, 1 min at 58°C, 2 min at 72°C; 35 cycles) of leaf DNA with the primer
536combination R498 and R490 for *GLD-T* (1943 bp) and T3 and T4 for *TRXo1* (min at 94°C, 1 min
537at 58°C, 2 min at 72°C; 35 cycles). For oligonucleotide sequences see Supp. Table 3.

538qRT-PCR expression analysis and immunological studies

539To extract total leaf RNA and protein, plant material (~100 mg) was harvested from air grown
540wild type and *trxo1-1* plants at growth stage 5.1 (Boyes et al., 2001) after 9 h of illumination or
541during the CO₂ transfer experiment (Fig. 2) and stored at -80°C until further processing. RNA
542isolation was carried out using the Nucleospin RNA plant kit (Macherey-Nagel). Following PCR
543verification of absence of DNA contamination, cDNA was synthesized from 2.5 µg of leaf RNA
544using the RevertAid cDNA synthesis kit (MBI Fermentas). Prior qRT-PCR analysis cDNA
545amounts were pre-calibrated by conventional RT-PCR using signals of the constitutively
546expressed 40S ribosomal protein *S16* gene. qRT-PCR of selected photorespiratory genes
547(*GLD-P1*, *GLD-T*, *GLD-H*, *GLD-L1*, *SHMT1*, *HPR1*, *pMDH1*, and *PGLP*; for sequences see
548Supp. Table 3) was performed on the LightCycler 1.5 system (Roche) and SYBR Green
549fluorescence (Roche) for detection as described previously (Timm et al., 2013). To obtain total
550leaf-protein, plant material was homogenized and extracted in 200 ml of extraction buffer
551containing 50 mM HEPES-KOH, pH 7.6, 10 mM NaCl, 5 mM MgCl₂, 100 mM sorbitol, and 0.1
552mM phenylmethylsulfonyl fluoride. After centrifugation (4°C, 10 min, 20,000g), the protein
553concentration of the supernatant was determined according to Bradford (1976). Subsequently,
55410 µg leaf proteins were separated via SDS page and transferred onto a PVDF membrane
555according to standard protocols. Antibodies of selected photorespiratory proteins (*pMDH1*, *GLD-*
556*P*, *GLD-T*, *GLD-H*, *GLD-L*, *SHMT1*, *HPR1*, and *PGLP*; Pracharoenwattana et al., 2007; Timm et
557al., 2013; Flügel et al., 2017) were used to estimate their abundances in the mutant lines and the
558wild type.

559Gas exchange and chlorophyll a fluorescence measurements

560Leaf gas exchange measurements were performed using fully expanded rosette leaves of plants
561at growth stage 5.1 (Boyes et al., 2001) with the following conditions: photon flux density = 1000
562µmol m⁻² s⁻¹, chamber temperature = 25°C, flow rate = 300 µmol s⁻¹, and relative humidity = 60 to
56370%. For A/C_i curves CO₂ steps were: 400, 300, 200, 100, 50, 0, and 400 ppm. Changes in the
564O₂ concentrations to 3, 40 or 50% (balanced with N₂), were generated via the gas-mixing system
565GMS600 (QCAL Messtechnik). Oxygen inhibition of A was calculated from measurements at 21
566and 50% oxygen using the equation: O₂ inhibition = (A₂₁ - A₅₀)/A₂₁*100. Calculation of γ was
567performed by linear regression of the Γ-versus-oxygen concentration curves and given as slopes
568of the respective functions. Simultaneously, chlorophyll a fluorescence was determined on a

569PAM fluorometer (DUAL-PAM-100; Walz). Maximum quantum yields of PSII were determined
570after dark adaptation of the plants for at least 15 min.

571Metabolite analysis

572For LC-MS/MS analysis, leaf material was harvested from fully expanded rosette leaves
573(sampling time points are specified in the legends of Fig. 2 and 6) of plants at growth stage 5.1
574(Boyes et al., 2001), immediately frozen in liquid nitrogen, and stored at -80°C until analysis.
575Extraction of soluble primary intermediates was carried out using LC-MS grade chemicals
576according to the method described in Arrivault et al., (2009; 2015) with some modifications.
577Briefly, ~50 mg leaf-tissue was grounded down to a fine powder and extracted in 500 µl of ice-
578cold LC-MS/MS buffer (150 µl chloroform, 350 µl methanol, 1 µl of 2-(N-
579Morpholino)ethanesulfonic acid (MES) as internal standard (1 mg/ml). Following addition of 400
580µl ice-cold water samples were vortexed thoroughly and incubated for at least 2 h at -20°C. After
581centrifugation (10 min, 20000 g, 4°C), the aqueous phase was transferred to new tube and 400
582µl of ice-cold water again added to the extraction tube. Following stirring and centrifugation (5
583min, 20000g, 4°C), supernatants were combined and lyophilized. Next, the dried extracts were
584dissolved in 400 µl water and filtrated through 0.2 µm filters (Omnifix®-F, Braun, Germany). The
585cleared supernatants were analyzed using the high performance liquid chromatograph mass
586spectrometer LCMS-8050 system (Shimadzu, Japan) and the incorporated LC-MS/MS method
587package for primary metabolites (version 2, Shimadzu, Japan). In brief, 1 µl of each extract was
588separated on a pentafluorophenylpropyl (PFPP) column (Supelco Discovery HS FS, 3 µm, 150 x
5892.1 mm) with a mobile phase containing 0.1% formic acid. The compounds were eluted at 0.25
590ml min⁻¹ using the following gradient: 1 min 0.1% formic acid, 95% A. *dest.*, 5% acetonitrile,
591within 15 min linear gradient to 0.1% formic acid, 5% A. *dest.*, 95% acetonitrile, 10 min 0.1%
592formic acid, 5% A. *dest.*, 95% acetonitrile. Aliquots were continuously injected in the MS/MS part
593and ionized via electrospray ionization (ESI). The compounds were identified and quantified
594using the multiple reaction monitoring (MRM) values given in the LC-MS/MS method package
595and the LabSolutions software package (Shimadzu, Japan). Authentic standard substances
596(Merck, Germany) at varying concentrations were used for calibration and peak areas
597normalized to signals of the internal standard. Glyoxylate, 3HP and glycerate were determined in
598the negative ion mode using selective ion monitoring (SIM) for *m/z* 73, 102 and 105
599corresponding to the deprotonated glyoxylate, 3HP and glycerate ions [M-H]⁻. Retention time
600acquisition window (2 min) was verified with co-elution experiments using purchased glyxoylate,
6013HP and glycerate (Sigma-Aldrich, Germany). Varying concentrations of the three metabolites

602 were also used for calibration curves. Data were interpreted using the Labsolution software
603 package (Shimadzu, Japan).

604 **Determination of pyridine nucleotide contents**

605 The contents of NAD⁺/NADH and NADP⁺/NADPH were determined in acid and alkaline extracts
606 using the protocol described in Queval and Noctor (2007). The assays involve the phenazine
607 methosulfate-catalyzed reduction of dichlorophenolindophenol (DCPIP) in the presence of
608 ethanol and alcohol dehydrogenase (for NAD⁺ and NADH) or glucose-6-P and glucose-6-P
609 dehydrogenase (for NADP⁺ and NADPH). Reduced and oxidized forms are distinguished by
610 preferential destruction through measurements in acid or alkaline buffers.

611

612 **Cloning, expression and purification of recombinant enzymes**

613 To express bacterial, cyanobacterial and plant LPDs the open reading frames were PCR
614 amplified from *E. coli* genomic DNA (*EcLPD*; MG1655; *EcLPD-S-BamHI/EcLPD-AS-Sall*),
615 *Synechocystis* sp. strain PCC 6803 genomic DNA (*SyLPD*; *slr1096*; 1096XhoI-fw/1096EcoRI-
616 rev) or *Pisum sativum* (*PsmtLPD*; P454/P294) cDNA and ligated into the pGEMT vector
617 (Invitrogen) for amplification and sequencing (Seqlab, Göttingen). The respective fragments
618 were excised using the introduced restriction sites (*EcLPD* – BamHI/Sall; *SyLPD* – XhoI/EcoRI
619 and *PsmtLPD* – BamHI/EcoRI) and ligated into vector pET28a (Novagene) or pBADHisA
620 (Invitrogen) to obtain pET28a-*EcLPD*, pBADHisA-*SyLPD* and pET28a-*PsmtLPD*. Expression
621 vectors pET16b-*AfTRXo1* and pET16b-*AfNTRa* were generated as described previously (Laloi
622 et al., 2001). Overexpression of the 4 constructs was carried out in 200 ml LB-medium
623 containing ampicillin (200 µg mL⁻¹) for the pBADHisA and pET16b or kanamycin (100 µg mL⁻¹)
624 for the pET28a vectors. Overexpression cultures were inoculated with 1 ml of a freshly prepared
625 overnight culture (~16 h) and shaken (200 rpm) at 37°C until OD₆₀₀ = ~0.6. Expression in
626 *Escherichia coli* was carried out as follows: pBADHisA:*SyLPD*, strain LMG194, induction with
627 0.2% (w/v) arabinose, and incubation at 30°C (200 rpm) for ~16 h or pET28a and pET16b, strain
628 BL21, induction with IPTG (1 mM), and incubation at 37°C (200 rpm) for 4 h (*EcLPD*, *AfTRXo1*
629 and *AfNTRa*) or 30°C for ~16 h (*PsmtLPD1*). The cells were harvested and resuspended in 20
630 mM TrisHCl, pH 8.0, containing 300 mM NaCl, and 20 mM Imidazol. Next, lysozyme was added
631 (1 mg/ml) and the crude extract incubated for 30 min on ice. The proteins were then extracted by
632 ultrasonic treatments (6 x 30 s, 90 W) in ice and centrifugation (20000g, 15 min, 4°C). To purify
633 recombinant *EcLDP*, *SyLPD*, *PsmtLPD*, *AfTRXo1* and *AfNTRa*, we performed nickel-

634nitrilotriacetic acid agarose affinity chromatography according to the protocol of the supplier
635(HisTrap; GE Healthcare). The eluted proteins were checked regarding purity using SDS-PAGE
636and staining by Coomassie Brilliant Blue and subsequently used for enzyme measurements.

637Isolation of mitochondria and mtLPD activity measurements

638To obtain mtLPD for activity measurements, mitochondria were isolated from ~50 g pea leaves
639according to Keech et al. (2005). Prior activity measurements mitochondria were solubilized by
640three freeze-thaw cycles, followed by 45 min centrifugation (40000g, 4°C). The obtained
641supernatant was used to determine the protein content. Total mtLPD activity in mitochondrial
642extracts or of recombinant proteins was assayed spectrophotometrically at 25°C (*Ps*LPD and
643*Sy*LPD) or 37°C (*Ec*LPD) as described previously (Timm et al., 2015). The reactions were
644initiated by adding 10-20 µg ml⁻¹ mitochondrial or 5-10 µg ml⁻¹ recombinant protein. Enzyme
645activity was determined without (control, oxidizing conditions) or after (reducing conditions)
646addition with 2 mM dithiothreitol (DTT) for 10 min at room temperature. Furthermore, the artificial
647proton donor DTT was exchanged with a native mitochondrial redox-system consisting of TRXo1
648and NTRa. Briefly, 30 µg NTRa and 12 µg TRXo1 were mixed with 100 µM NADPH in 100 µl
649potassium-phosphate, incubated for at least 10 min at 25°C and after addition of all other
650components of the test, mtLPD activity was monitored at 340 nm. For control measurements, the
651same reactions were carried out after boiling of TRXo1 and NTRa for 10 min at 90°C.

652Statistical analysis

653Significant values were determined using the two-tailed Student's *t* test (Microsoft Excel 10.0)
654and by ANOVA for multiple genotypes using the Holm and Sidak test for comparisons (Sigma
655Plot 11; Systat Software). The term significant is used here only if the change in question has
656been confirmed to be significant at the level of **p* < 0.05 or ***p* < 0.01.

657Accession numbers

658The Arabidopsis Genome Initiative or GenBank/EMBL database contains sequence data from
659this article under the following accession numbers: TRXo1 (At2g35010), NTRa (At2g17420),
660GDC-T (At1g11680), GDC-P1 (At4g33010), GDC-H1 (At1g32470), GDC-L1 (mtLPD1)
661(At1g48030), GDC-L2 (AT3G17240), SHMT1 (At4g37930), pMDH (At2g22780), HPR1
662(At1g68010), PGLP1 (At5g35700), ODGC-E2 (At5g55070), PDC-E2 (At3g52200), RbcL
663(ATCG00490), 40S ribosomal protein S16 (At2g09990), pea LPD (P31023), maize LPD

664(A0A1D6MSE3), Syn LPD (P72740), *E.coli* LPD (P0A9P0), *Azotobacter vinelandii* LPD
665(C1DGW2) and *Pseudomonas putida* LPD (Q88C17).

666Author Contributions

667S.T. conceived and supervised the project. O.R., S.S., Y.Z. and S.T. performed the research and
668analyzed data. J.P.R. provided expression clones for TRXo1 and NTRa and A.R.F. the T-DNA
669insertional mutant *trxo1-1*. A.R.F. and M.H. provided experimental equipment and tools. S.T.
670wrote the article, with additions and revisions from all authors. All authors have read and
671approved the final version of the manuscript.

672Acknowledgements

673We wish to thank Maria Wittmiß (Rostock) for introducing O.R. in enzymatic measurements and
674providing recombinant LPD of Synechocystis PCC6803 and the Nottingham Arabidopsis Stock
675Centre for the T-DNA insertional lines. We also acknowledge the technical assistance from Ina
676Krahnert (Potsdam-Golm). The donation of antibodies received from Hermann Bauwe
677(University of Rostock, Germany) and Steven M. Smith (University of Tasmania, Australia) has
678facilitated the study. This work was financially supported by the University of Rostock (to M.H.
679and S.T.). The LC-MS equipment at the University of Rostock was financed through the HBF
680program (GZ: INST 264/125-1 FUGG). This study is set within the framework of the
681"Laboratoires d'Excellences (LABEX)" TULIP (ANR-10-LABX-41).

682Supplemental Data

683**Supplemental Table 1.** Absolute metabolite contents in *trxo1* and the wild type during CO₂
684transition.

685**Supplemental Table 2.** Absolute metabolite contents in *trxo1*, *gldt1* and *TxGT* compared to the
686wild type grown in HC and LC conditions.

687**Supplemental Table 3.** Oligonucleotides used during this study.

688**Supplemental Figure 1.** Phenotype and PCR verification of the *TxGT* double mutant.

689Supplemental Figure 2. Expression of selected photorespiratory and TCA cycle enzymes during
690CO₂ transition.

691Supplemental Figure 3. Alignment of LPD proteins from different sources.

692Supplemental Figure 4. 3D protein structure models of pea, Synechocystis and *E.coli* LPD.

693

6941

6952

696 Literature cited

697 **Alonso JM, Stepanova AN, Leisse TJ, Kim CJ, Chen H, Shinn P, Stevenson DK,**
698 **Zimmerman J, Barajas P, Cheuk R, Gadrinab C, Heller C, Jeske A, Koesema E, Meyers**
699 **CC, Parker H, Prednis L, Ansari Y, Choy N, Deen H, Geralt M, Hazari N, Hom E, Karnes M,**
700 **Mulholland C, Ndubaku R, Schmidt I, Guzman P, Aguilar-Henonin L, Schmid M, Weigel D,**
701 **Carter DE, Marchand T, Risseeuw E, Brogden D, Zeko A, Crosby WL, Berry CC, Ecker JR**
702 (2003) Genome-wide insertional mutagenesis of *Arabidopsis thaliana*. *Science* **301**: 653-657

703 **Anderson LE** (1971) Chloroplast and cytoplasmic enzymes. II. Pea leaf triose phosphate
704 isomerases. *Biochimica et Biophysica Acta* **235**: 237–244

705 **Appel AM, Bercaw JE, Bocarsly AB, Dobbek H, DuBois DL, Dupuis M, Ferry JG, Fujita E,**
706 **Hille R, Kenis PJA, Kerfeld CA, Morris RH, Peden CHF, Portis AR, Ragsdale SW,**
707 **Rauchfuss TB, Reek JNH, Seefeldt LC, Thauer RK, Waldrop GL.** (2013) Frontiers,
708 Opportunities, and Challenges in Biochemical and Chemical Catalysis of CO₂ Fixation. *Chemical*
709 *Reviews* **113**: 6621-6658

710 **Arrivault S, Guenther M, Ivakov A, Feil R, Vosloh D, van Dongen JT, Sulpice R, Stitt M**
711 (2009) Use of reverse-phase liquid chromatography, linked to tandem mass spectrometry, to
712 profile the Calvin cycle and other metabolic intermediates in *Arabidopsis* rosettes at different
713 carbon dioxide concentrations. *Plant Journal* **5**: 826–39

714 **Arrivault, S, Guenther, M, Fry, SC, Fuenfgeld, MMFF, Veyel, D, Mettler-Altmann, T, Stitt, M,**
715 **Lunn, JE** (2015) Synthesis and use of stable-isotope-labeled internal standards for
716 quantification of phosphorylated metabolites by LC-MS/MS. *Analytical Chemistry* **87**: 6896–
717 6904.

718 **Badger MR, Fallahi H, Kaines S, Takahashi S** (2009) Chlorophyll fluorescence screening
719 of *Arabidopsis thaliana* for CO₂ sensitive photorespiration and photoinhibition mutants.
720 *Functional Plant Biology* **36**: 867-873

721 **Balmer Y, Vensel WH, Tanaka CK, Hurkman WJ, Gelhaye E, Rouhier N, Jacquot JP,**
722 **Manieri W, Schürmann P, Droux M, Buchanan B** (2004) Thioredoxin links redox to the
723 regulation of fundamental processes of plant mitochondria. *Proc. Natl. Acad. Sci. USA* **101**:
724 2642–2647

725

726 **Bauwe H, Hagemann M, Fernie AR** (2010) Photorespiration: players, partners and origin.
727 *Trends in Plant Science* **15**: 330-336

728 **Bauwe H, Hagemann M, Kern R, Timm S** (2012) Photorespiration has a dual origin and
729 manifold links to central metabolism. *Current Opinion in Plant Biology* **15**: 269-275

730 **Betti M, Bauwe H, Busch FA, Fernie AR, Keech O, Levey M, Ort DR, Parry MAJ, Sage R,**
731 **Timm S, Walker B, Weber APM** (2016) Manipulating photorespiration to increase plant
732 productivity: recent advances and perspectives for crop improvement. *Journal of Experimental*
733 *Botany* **67**: 2977-2988

734 **Blackwell RD, Murray AJS, Lea PJ, Kendall AC, Hall NP, Turner JC, Wallsgrove RM** (1988)
735 The value of mutants unable to carry out photorespiration. *Photosynthesis Research* **16**: 155-
736 176

737 **Bradford MM** (1976) A rapid and sensitive method for the quantitation of microgram quantities
738 of protein utilizing the principle of protein-dye binding. *Anal Biochem* **72**: 248-254

739 **Bourguignon J, Neuburger M, Douce R** (1988) Resolution and characterization of the glycine
740 cleavage reaction in pea leaf mitochondria. Properties of the forward reaction catalysed by
741 glycine decarboxylase and serine hydroxymethyltransferase. *Biochemical Journal* **255**: 169-78

742 **Bowes G, Ogren WL, Hageman RH** (1971) Phosphoglycolate production catalyzed by ribulose
743 diphosphate carboxylase. *Biochemical and Biophysical Research Communications* **45**: 716-722

744 **Boyes DC, Zayed AM, Ascenzi R, McCaskill AJ, Hoffman NE, Davis KR, Gorkach J** (2001)
745 Growth stage-based phenotypic analysis of Arabidopsis: A model for high throughput functional
746 genomics in plants. *Plant Cell* **13**: 1499-1510

747

748 **Carroll AJ, Zhang P, Withehead L, Kaines S, Tcherkez G, Badger MJ** (2015) PhenoMeter: a
749 metabolome database search tool using statistical similarity matching of metabolic phenotypes
750 for high-confidence detection of functional links. *Frontiers in Bioengineering and Biotechnology*
751 <https://doi.org/10.3389/fbioe.2015.00106>

752 **Cousins AB, Walker BJ, Pracharoenwattana I, Smith SM, Badger MR** (2011) Peroxisomal
753 hydroxypyruvate reductase is not essential for photorespiration in Arabidopsis but its absence
754 causes an increase in the stoichiometry of photorespiratory CO₂ release. *Photosynthesis*
755 *Research* **108**: 91-100

756**Daloso, DM, Müller K, Obata T, Florian A, Tohge T, Bottcher A, Riondet C, Bariat L, Carrari**
757**F, Nunes-Nesi A, Buchanan BB, Reichheld J-P, Araújo WL, Fernie AR (2015)** Thioredoxin, a
758master regulator of the tricarboxylic acid cycle in plant mitochondria. Proceedings of the National
759Academy of Sciences of the United States of America, **112**: 1392-1400

760**Dellero Y, Lamothe-Sibold M, Jossier M, Hodges M (2015)** Arabidopsis thaliana ggt1
761photorespiratory mutants maintain leaf carbon:nitrogen balance by reducing RuBisCO content
762and plant growth. The Plant Journal **83**: 1005-1018

763**Douce R, Bourguignon J, Besson V, Macherel D, Neuburger M (1991)** Structure and function
764of the glycine cleavage complex in green leaves. In: Huang AHC, Taiz L, eds. Molecular
765approaches to compartmentation and metabolic regulation. Rockville: American Society of Plant
766Physiologists, 59-73.

767**Douce R, Bourguignon J, Neuburger M, Rébeillé F (2001)** The glycine decarboxylase system:
768a fascinating complex. Trends Plant Science **6**: 167–176

769**Eisenhut M, Ruth W, Haimovich M, Bauwe H, Kaplan A, Hagemann M (2008)** The
770photorespiratory glycolate metabolism is essential for cyanobacteria and might have been
771conveyed endosymbiotically to plants. Proceedings of the National Academy of Sciences, USA
772**105**: 17199–17204

773**Eisenhut M, Planchais S, Cabassa C et al. (2013a)** Arabidopsis A BOUT DE SOUFFLE is a
774putative mitochondrial transporter involved in photorespiratory metabolism and is required for
775meristem growth at ambient CO₂ levels. The Plant Journal **73**: 836-849

776

777**Eisenhut M, Bräutigam A, Timm S, Florian A, Tohge T, Fernie AR, Bauwe H, Weber**
778**A (2016)** Photorespiration is crucial to the dynamic response of photosynthetic metabolism to
779altered CO₂ availability. Molecular Plant **10**: 47-61

780**Faure M, Bourguignon J, Neuburger M, Macherel D, Sieker L, Ober R, Kahn R, Cohen-**
781**Addad C, Douce R (2000)** Interaction between the lipoamide-containing H-protein and the
782lipoamide dehydrogenase (L-protein) of the glycine decarboxylase multienzyme system 2.
783Crystal structures of H- and L-proteins. Eur. J. Biochem. **267**: 2890-2898

784**Fernie A, Bauwe H, Eisenhut M, Florian A, Hanson D, Hagemann M, Keech O, Mielewczik**
785**M, Nikoloski Z, Peterhänsel C, Roje S, Sage R, Timm S, von Caemmerer S, Weber A,**

786**Westhoff P** (2013) Perspectives on plant photorespiratory metabolism. *Plant Biology* **45**: 748-787753

788**Flügel F, Timm S, Arrivault S, Florian A, Stitt M, Fernie AR, Bauwe H** (2017) The
789Photorespiratory Metabolite 2-Phosphoglycolate Regulates Photosynthesis and Starch
790Accumulation in Arabidopsis. *The Plant Cell* **29**: 2537-2551

791**Foyer CH, Bloom AJ, Queval G, Noctor G** (2009) Photorespiratory metabolism: genes,
792mutants, energetics, and redox signaling. *Annual Reviews in Plant Biology* **60**: 455-484

793**Geigenberger P, Thormählen I, Daloso DM, Fernie A.R.** (2017) The unprecedented versatility
794of the plant thioredoxin system. *Trends in Plant Science* **22**: 249–262

795**Hasse D, Andersson E, Carlsson G, Masloboy A, Hagemann M, Bauwe H, Andersson I**
796(2013) Structure of the homodimeric glycine decarboxylase P-protein from *Synechocystis* sp.
797PCC 6803 suggests a mechanism for redox regulation. *Journal of Biological Chemistry* **288**:
79835333-35345

799**Hodges M, Jossier M, Boex-Fontvieille E, Tcherkez G** (2013) Protein phosphorylation and
800photorespiration. *Plant Biology* **15**: 694–706

801**Hodges M, Dello Y, Keech O, Betti M, Raghavendra AS, Sage R, Zhu XG, Allen DK,**
802**Weber AP** (2016) Perspectives for a better understanding of the metabolic integration of
803photorespiration within a complex plant primary metabolism network. *Journal of Experimental*
804*Botany* **67**: 3015–3026

805**Hodges M, Jossier M, Boex-Fontvieille E, Tcherkez G** (2013) Protein phosphorylation and
806photorespiration. *Plant Biology* **15**: 694–706

807**Hoffmann C, Plochanski B, Haferkamp I, Leroch M, Ewald R, Bauwe H, Riemer J,**
808**Herrmann J, Neuhaus E** (2013) From endoplasmic reticulum to mitochondria: Absence of the
809Arabidopsis ATP antiporter ER-ANT1 perturbs photorespiration. *The Plant Cell* **25**: 2647-2660

810**Keech O, Dizengremel P, Gardeström P** (2005) Preparation of leaf mitochondria from
811Arabidopsis thaliana. *Physiol Plant* **124**: 403–409

812

813**Keech O, Gardeström P, Kleczkowski LA, Rouhier N** (2017) The redox control of
814photorespiration: from biochemical and physiological aspects to biotechnological considerations.
815*Plant Cell Environment* **40**: 553-569

816**Kelly GJ, Latzko E** (1976) Inhibition of spinach-leaf phosphofructokinase by 2-
817phosphoglycollate. FEBS Letters **68**: 55–58

818**Laloi C, Rayapuram N, Chartier Y, Grienenberger JM, Bonnar G, Meyer Y** (2001)
819Identification and characterization of a mitochondrial thioredoxin system in plants. Proceedings
820of the National Academy of Sciences of the United States of America, 98: 14144-14149

821**Li J, Weraduwage SM, Peiser AL, Tietz S, Weise SE, Strand DD, Froehlich JE, Kramer**

822**DM, Hu J, Sharkey TD** (2019) A Cytosolic Bypass and G6P Shunt in Plants Lacking

823Peroxisomal Hydroxypyruvate Reductase. Plant Physiology

824DOI:<https://doi.org/10.1104/pp.19.00256>

825**Leegood RC, Lea PJ, Adcock MD, Häusler RE** (1995) The regulation and control of
826photorespiration. Journal of Experimental Botany **46**: 1397-1414

827**Levey M, Timm S, Mettler-Altmann T, Borghi GL, Koczor M, Arrivault S, Weber APM,**

828**Bauwe H, Gowik U, Westhoff P** (2019) Efficient 2-phosphoglycolate degradation is required to

829maintain carbon assimilation and allocation in the C₄ plant *Flaveria bidentis*. Journal of

830Experimental Botany, **70**: 575-587

831**López-Calcagno PE, Fisk S, Brown KL, Bull SE, South PF, Raines CA** (2018)

832Overexpressing the H-protein of the glycine cleavage system increases biomass yield in

833glasshouse and field-grown transgenic tobacco plants. Plant Biotechnology Journal doi:

83410.1111/pbi.12953

835

836**Millar AH, Knorrpp C, Leaver CJ, Hill SA** (1998) Plant mitochondrial pyruvate dehydrogenase

837complex: purification and identification of catalytic components in potato. Biochemical Journal

838**334**: 571–576

839**Nakamura Y, Kanakagiri S, Van K, He W, Spalding MH** (2005) Disruption of the glycolate

840dehydrogenase gene in the high-CO₂-requiring mutant HCR89 of *Chlamydomonas reinhardtii*.

841Canadian Journal of Botany **83**: 820–833

842**Obata T, Florian A, Timm S, Bauwe H, Fernie AR** (2016) On the metabolic interaction of

843(photo)respiration. Journal of Experimental Botany **67**: 3003-3014

844**Ogren WL, Bowes G** (1971) Ribulose diphosphate carboxylase regulates soybean

845photorespiration. Nature New Biology **230**: 159–160

846**Oliver DJ, Sarojini G** (1987) Regulation of glycine decarboxylase by serine. In: Biggins J, ed.
847Progress in photosynthesis research, Vol. III. Dordrecht: Martinus Nijhoff, 573-6.

848**Oliver DJ, Neuburger M, Bourguignon J, Douce R** (1990) Interaction between the component
849enzymes of the glycine decarboxylase multienzyme complex. *Plant Physiology* **94**: 833–839

850**Orf I, Timm S, Bauwe H, Fernie AR, Hagemann M, Kopka J, Nikoloski Z** (2016) Can
851cyanobacteria serve as a model of plant photorespiration? – A comparative analysis of
852metabolite profiles. *Journal of Experimental Botany* **67**: 2941-2952

853**Palmieri MC, Lindermayr C, Bauwe H, Steinhauser C, Durner J** (2010) Regulation of Plant
854Glycine Decarboxylase by S-Nitrosylation and Glutathionylation. *Plant Physiology* **152**: 1514-
8551528

856**Peterhänsel C, Krause K, Braun H-P, Espie GS, Fernie AR, Hanson DT, Keech O, Maurino**
857**VG, Mielewczik M, Sage RF** (2013) Engineering photorespiration: current state and future
858possibilities. *Plant Biology* **15**: 754–758

859**Pérez-Pérez ME, Mauriès A, Maes A, Tourasse NJ, Hamon M, Lemaire SD, et al.** (2017) The
860deep thioredoxome in *Chlamydomonas reinhardtii*: new insights into redox regulation. *Molecular*
861*Plant* **10**: 1107–1125

862**Pick TR, Bräutigam A, Schulz MA, Obata T, Fernie AR, Weber APM** (2013) PLGG1, a
863plastidic glycolate glycerate transporter, is required for photorespiration and defines a unique
864class of metabolite transporters. *Proceedings of the National Academy of Sciences of the United*
865*States of America* **110**: 3185-3190

866**Pracharoenwattana I, Cornah JE, Smith SM** (2007) Arabidopsis peroxisomal malate
867dehydrogenase functions in β -oxidation but not in the glyoxylate cycle. *The Plant Journal*, **50**:
868381-390

869**Queval G, Noctor G** (2007) [A plate reader method for the measurement of NAD, NADP,](#)
870[glutathione, and ascorbate in tissue extracts: application to redox profiling during Arabidopsis](#)
871[rosette development.](#) *Anal Biochem* **363**: 58–69

872**Rademacher N, Kern R, Fujiwara T, Mettler-Altmann T, Miyagishima SY, Hagemann M,**
873**Eisenhut M, Weber AP** (2016) Photorespiratory glycolate oxidase is essential for the survival of
874the red alga *Cyanidioschyzon merolae* under ambient CO₂ conditions. *Journal of Experimental*
875*Botany* **67**: 3165–3175

876**Reichheld JP, Khafif M, Riondet C, Droux M, Bonnard G, Meyer Y** (2007) Inactivation of
877thioredoxin reductases reveals a complex interplay between thioredoxin and glutathione
878pathways in Arabidopsis development. *Plant Cell* **19**: 1851-1865

879**Reumann S, Weber APM** (2006) Plant peroxisomes respire in the light: Some gaps of the
880photorespiratory C2-cycle have become filled – Others remain. *Biochimica et Biophysica Acta*
881**1763**: 1496-1510

882

883

884

885**Simkin A, Lopez-Calcagno P, Davey P, Headland L, Lawson T, Timm S, Bauwe H, Raines**
886**C** (2017) Simultaneous stimulation of the SBPase, FBP aldolase and the photorespiratory GDC-
887H protein increases CO₂ assimilation, vegetative biomass and seed yield in Arabidopsis. *Plant*
888*Biotechnology Journal* **15**: 805-816

889**Somerville CR** (2001) An early Arabidopsis demonstration. Resolving a few issues concerning
890photorespiration. *Plant Physiology* **125**: 20–24

891**Somerville CR, Ogren WL** (1979) Phosphoglycolate phosphatase-deficient mutant of
892Arabidopsis. *Nature* **280**: 833-836

893**South PF, Cavanagh AP, Lopez-Calcagno PE, Raines CA, Ort DR** (2018) Optimizing
894photorespiration for improved crop productivity. *Journal of Integrative Plant Biology* doi: 10.1111/
895jipb.12709

896**South PF, Cavanagh AP, Liu HW, Ort DR** (2019) [Synthetic glycolate metabolism pathways](#)
897[stimulate crop growth and productivity in the field.](#) *Science* **363** (6422). doi:
89810.1126/science.aat9077

899**Suzuki K, Marek LF, Spalding MH** (1989) A photorespiratory mutant of *Chlamydomonas*
900*reinhardtii*. *Plant Physiology* **93**: 231–237

901**Taylor NL, Day DA, Millar AH** (2002) Environmental stress causes oxidative damage to plant
902mitochondria leading to inhibition of glycine decarboxylase. *The Journal of Biological Chemistry*
903**277**: 42663–42668

904 **Timm S, Florian A, Jahnke K, Nunes-Nesi A, Fernie AR, Bauwe H** (2011) The
905 hydroxypyruvate-reducing system in Arabidopsis: multiple enzymes for the same end. *Plant*
906 *Physiology* **155**: 694–705

907 **Timm S, Mielewczik M, Florian A, Frankenbach S, Dreissen A, Hocken N, Fernie AR,**
908 **Walter A, Bauwe H** (2012a) High-to-low CO₂ acclimation reveals plasticity of the
909 photorespiratory pathway and indicates regulatory links to cellular metabolism of Arabidopsis.
910 *PLoS ONE* **7**, e42809.

911 **Timm S, Florian A, Arrivault S, Stitt M, Fernie AR, Bauwe H** (2012b) Glycine decarboxylase
912 controls photosynthesis and plant growth. *FEBS Letters* **586**: 3692-3697

913 **Timm S, Bauwe H** (2013) The variety of photorespiratory phenotypes - employing the current
914 status for future research directions on photorespiration. *Plant Biology* **15**: 737-747.

915 **Timm S, Florian A, Wittmiß M, Jahnke K, Hagemann M, Fernie AR, Bauwe H** (2013) Serine
916 acts as metabolic signal for the transcriptional control of photorespiration-related genes
917 in *Arabidopsis thaliana*. *Plant Physiology* **162**: 379-389

918 **Timm S, Wittmiß M, Gamlien S, Ewald R, Florian A, Frank M, Wirtz M, Hell R, Fernie AR,**
919 **Bauwe H** (2015) Mitochondrial dihydrolipoyl dehydrogenase activity shapes photosynthesis and
920 photorespiration of *Arabidopsis thaliana*. *The Plant Cell* **27**: 1968-1984

921 **Timm S, Florian A, Fernie AR, Bauwe H** (2016) The regulatory interplay between
922 photorespiration and photosynthesis. *Journal of Experimental Botany* **67**: 2923-2929

923

924 **Timm S, Giese J, Engel N, Wittmiß M, Florian A, Fernie AR, Bauwe H** (2018) T-protein is
925 present in large excess over the other proteins of the glycine cleavage system in leaves of
926 Arabidopsis. *Planta* **1**: 41-51

927 **Tolbert NE** (1971) Microbodies Peroxisomes and glyoxysomes. *Annual Reviews in Plant*
928 *Physiology* **22**: 45–74

929 **Walker JL, Oliver DJ** (1986) Light-induced increases in the glycine decarboxylase multienzyme
930 complex from pea leaf mitochondria. *Archives of Biochemistry and Biophysics* **248**: 626-638

931 **Walker BJ, VanLoocke A, Bernacchi CJ, Ort DR** (2016) The costs of photorespiration to food
932 production now and in the future. *Annual Review of Plant Biology* **67**: 107- 129

933**Wingler A, Lea PJ, Quick WP, Leegood RC** (2000) Photorespiration: metabolic pathways and
934their role in stress protection. *Philos. Trans. R. Soc. London Ser. B* **355**: 1517–29

935**Woody ST, Austin-Phillips S, Amasino RM, Krysan PJ** (2007) The *WiscDsLox* T-DNA
936collection: an arabidopsis community resource generated by using an improved high-throughput
937T-DNA sequencing pipeline. *J Plant Res* **120**: 157-165

938**Vauclare P, Diallo N, Bourguignon J, Macherel D, Douce R** (1996) Regulation of the
939Expression of the Glycine Decarboxylase Complex during Pea Leaf Development. *Plant*
940*Physiology* **112**: 1523-1530

941

942**Zelitch I** (1964) Organic acids and respiration in photosynthetic tissues. *Annual Reviews in Plant*
943*Physiology* **15**: 121–142

944**Zelitch I, Schultes NP, Peterson RB, Brown P, Brutnell TP** (2009) High glycolate oxidase
945activity is required for survival of maize in normal air. *Plant Physiology* **149**: 195–204

946**Zhang X, Zheng X, Ke S, Zhu H, Liu F, Zhang Z, Peng X, Guo L, Zeng R, Hou P, Liu Z, Wu**
947**S, Song M, Yang J, Zhang G** (2016) ER-localized adenine nucleotide transporter ER-ANT1: an
948integrator of energy and stress signaling in rice. *Plant Molecular Biology* **92**: 701-715

949

950 **Figure legends**

951 **Figure 1. Oxygen-dependent gas exchange of *trxo1* and the wild type.**

952 Plants were grown in normal air (390 ppm CO₂) with a 10/14 h day/night cycle. After 8 weeks
953 (growth stage 5.1, Boyes et al., 2001), plants were used for gas exchange measurements at
954 varying oxygen concentrations (3%, 21%, 40%, and 50%, balanced with N₂). Mean values ± SD
955 (n = 5-8) are shown for **(A)** net CO₂ uptake rates (A) and oxygen inhibition of A and **(B)** CO₂
956 compensation points (Γ) and slopes of the Γ-versus-oxygen concentrations (γ). Asterisks
957 indicate significant alterations of the *trxo1* mutant to the wild type according to Student's *t*-test
958 (*p < 0.05, **p < 0.01, n.s. – not significant). For details on the calculation of oxygen inhibition
959 and γ see material and methods section.

960 **Figure 2. Selected metabolites in wild type, *trxo1* and *gldt1* plants during CO₂ transition.**

961 Plants were grown in high CO₂ (1500 ppm, HC) with a 10/14 h day/night cycle. After 8 weeks
962 (growth stage 5.1, Boyes et al., 2001) plants were transferred in normal air (390 CO₂) with
963 otherwise equal conditions. Leaf-material was harvested in HC (9 h light) and in normal air (1
964 and 9 h light), respectively. Shown are mean values ± SD (n = 6) of selected metabolites
965 quantified by LC-MS/MS analysis. For a more comprehensive dataset including statistical
966 evaluation please compare Supp. Datasheet 1.

967 **Figure 3. Expression of selected photorespiratory enzymes on the mRNA and protein** 968 **level.**

969 Plants were grown in normal air (390 ppm CO₂) with a 10/14 h day/night cycle. After 8 weeks
970 (growth stage 5.1, Boyes et al., 2001), leaf-material was harvested at the end of the day (9 h
971 illumination) and used for subsequent mRNA and protein extraction. Shown are mean values ±
972 SD (n = 3) of mRNA expression and representative immunoblots from the *trxo1* mutant
973 compared to the control (n.s. – not significant; n.d. – not determined).

974 **Figure 4. Phenotype, growth and chlorophyll a fluorescence of the *TxGT* double mutant.**

975 Plants were grown in **(A)** normal air (390 ppm CO₂) or **(B)** high CO₂ (1500 ppm, HC) with a
976 10/14 h day/night cycle. After 5 weeks plants were photographed, rosette diameters and total
977 leaf-numbers determined and chl a fluorescence measurements carried out. Shown are mean
978 values ± SD (n > 5). Asterisks indicate values significantly different from the control (*p < 0.05;

979**p < 0.01; n.s. – not significant) and plusses between the *gldt1* single and the *TxGT* double
980mutant (⁺p < 0.05).

981**Figure 5. Oxygen-dependent gas exchange of *gldt1*, *TxGT* and the wild type.**

982Plants were grown in high CO₂ (1500 ppm) with a 10/14 h day/night cycle. After 7 weeks (growth
983stage 5.1, Boyes et al., 2001), plants were transferred to normal air (390 ppm CO₂) and used for
984gas exchange measurements at varying oxygen concentrations (3%, 21%, and 50%, balanced
985with N₂) after one week acclimation to the altered atmosphere. Mean values ± SD (n = 5-8) are
986shown for **(A)** net CO₂ uptake rates (A) and oxygen inhibition of A and **(B)** CO₂ compensation
987points (Γ) and slopes of the Γ-versus-oxygen concentrations (γ). Asterisks indicate significant
988alterations of the mutants to the wild type according to Student's *t*-test (*p < 0.05, **p < 0.01) and
989plusses between the *gldt1* single and the *TxGT* double mutant (⁺p < 0.05). For details on the
990calculation of oxygen inhibition and γ see material and methods section.

991**Figure 6. Pyridine nucleotide contents in wild type, *gldt1*, *trxo1* and *TxGT* plants during
992CO₂ transition.**

993Plants were grown in high CO₂ (1500 ppm, HC) with a 10/14 h day/night cycle. After 8 weeks
994(growth stage 5.1, Boyes et al., 2001) plants were transferred in normal air (390 ppm CO₂) with
995otherwise equal conditions. Leaf-material was harvested in HC (9 h light) and in normal air (1
996and 9 h light), respectively. Shown are mean values ± SD (n > 6) of pyridine nucleotides (NAD⁺,
997NADH, NADP⁺ and NADPH) quantified by spectrophotometric analysis. Asterisks indicate
998significant alterations of the mutants to the wild type according to Student's *t*-test (*p < 0.05, **p
999< 0.01, n.s. – not significant).

1000**Figure 7. Levels of selected metabolites in leaves of the wild type, *trxo1*, *gldt1* and *TxGT*
1001mutants grown in HC and normal air.**

1002Plants were grown in high CO₂ (1500 ppm, HC) and normal air (390 ppm CO₂) with a 10/14 h
1003day/night cycle. After 8 weeks (growth stage 5.1, Boyes et al., 2001), leaf-material was
1004harvested in both conditions after 9 h illumination. Shown are mean values ± SD (n > 4) of
1005selected metabolites quantified by LC-MS/MS analysis. Asterisks indicate significant alterations
1006of the mutants to the wild type in each condition according to Student's *t*-test (*p<0.05; **p<0.01)
1007and plusses between HC and normal air values of each genotype (*p<0.05). For a more
1008comprehensive dataset including statistical evaluation please compare Supp. Datasheet 2.

1009 **Figure 8. Redox-regulation of mtLPD1 from pea and Synechocystis.**

1010 The activity of mtLPD was determined in **(A)** pea leaf-mitochondria and from recombinant **(B)**
1011 pea and **(C)** Synechocystis proteins, respectively. Shown are mean values \pm SD ($n > 4$) of
1012 mtLPD activity without or after addition of DTT and recombinant native or boiled TRXo1 and
1013 NTRa as described in detail in the material and methods section. Asterisks indicate significant
1014 alterations to the control according to Student's *t*-test (* $p < 0.05$, ** $p < 0.01$, n.s. – not
1015 significant).

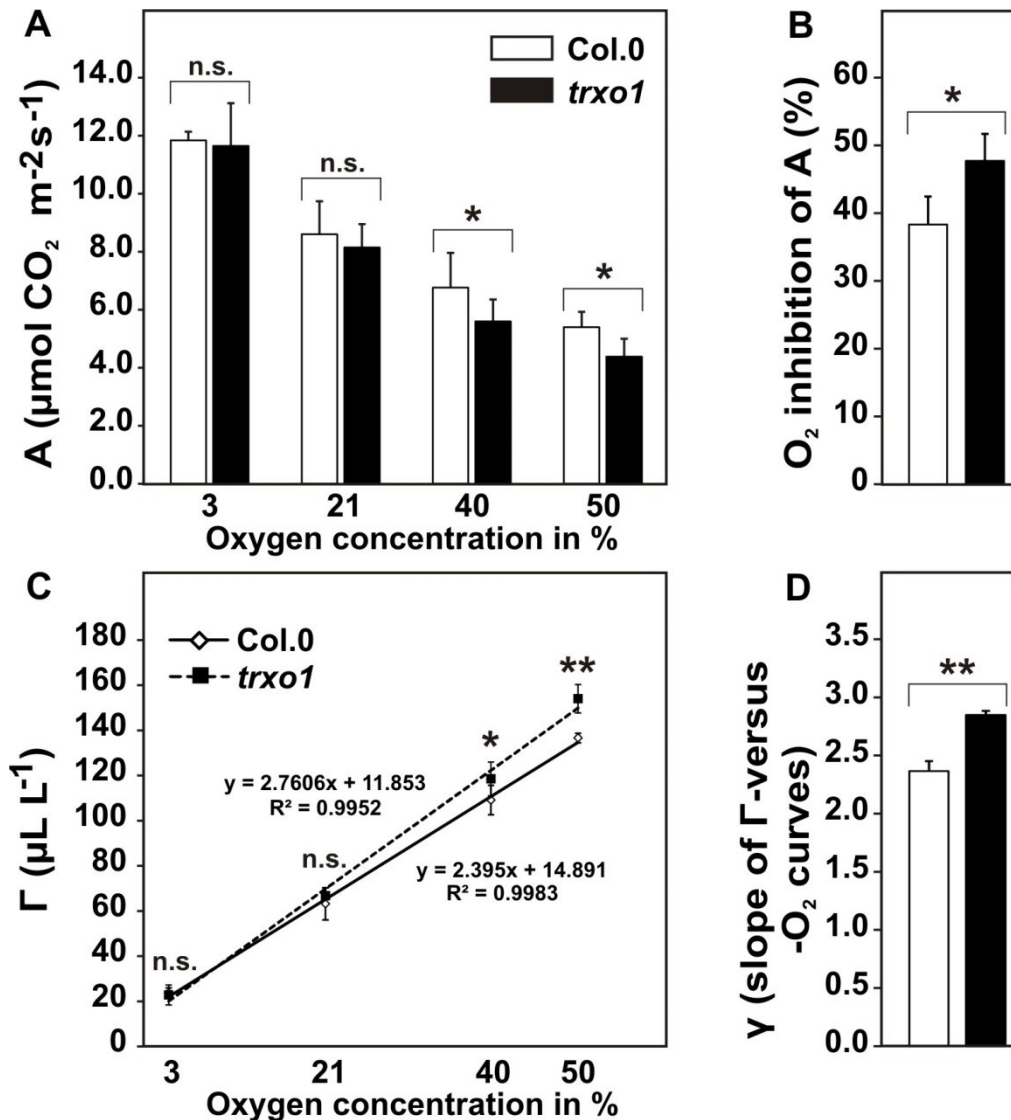


Figure 1. Oxygen-dependent gas exchange of *trxo1* and the wild type.

Plants were grown in normal air (390 ppm CO₂) with a 10/14 h day/night cycle. After 8 weeks (growth stage 5.1, Boyes et al., 2001), plants were used for gas exchange measurements at varying oxygen concentrations (3%, 21%, 40%, and 50%, balanced with N₂). Mean values ± SD (n = 5-8) are shown for **(A)** net CO₂ uptake rates (A) and **(B)** oxygen inhibition of A and **(C)** CO₂ compensation points (Γ) and **(D)** slopes of the Γ-versus-oxygen concentrations (γ). Asterisks indicate significant alterations of the *trxo1* mutant to the wild type according to Student's *t*-test (*p < 0.05, **p < 0.01, n.s. – not significant). For details on the calculation of oxygen inhibition and γ see material and methods section.

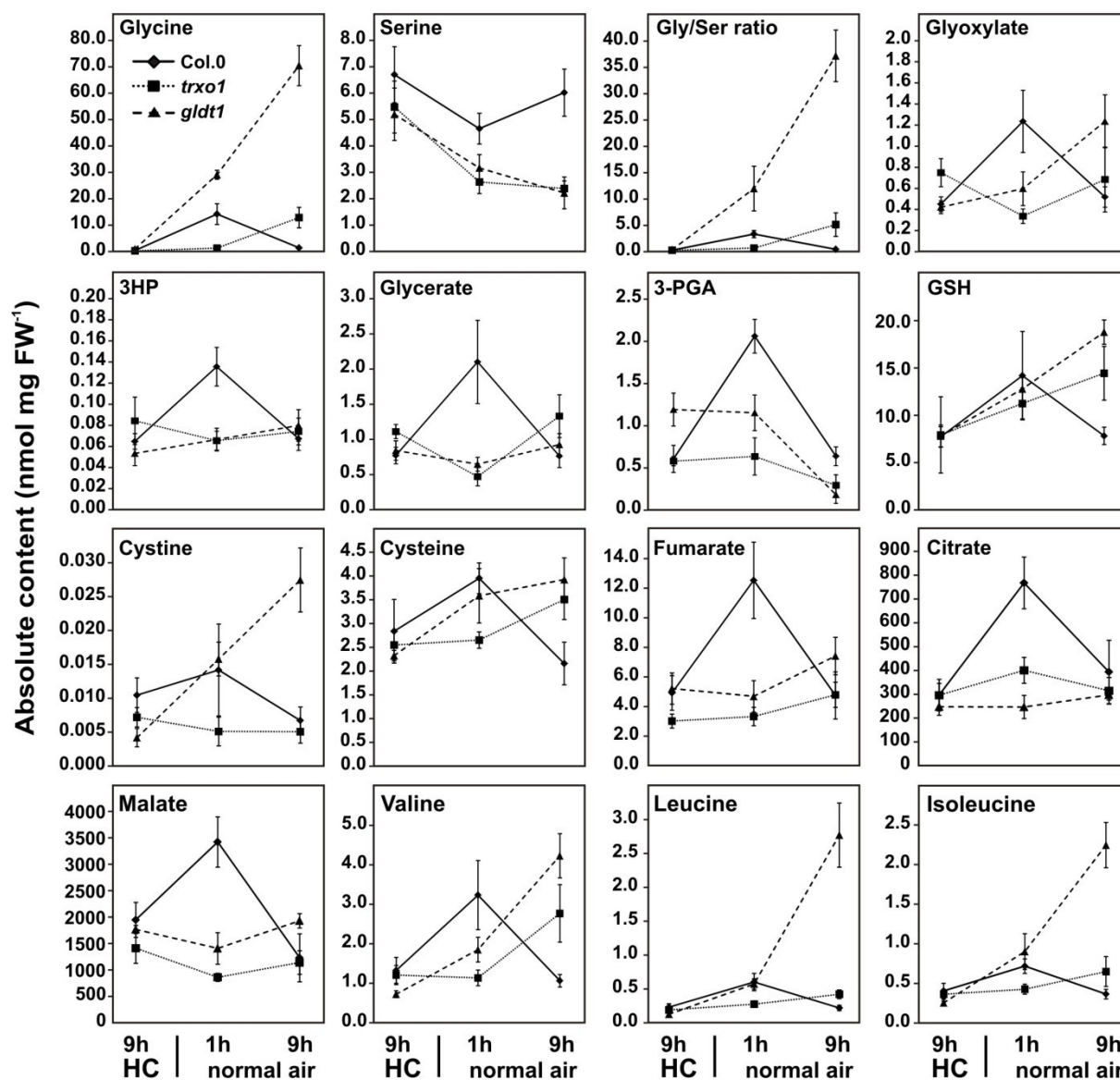


Figure 2. Selected metabolites in wild type, *trxo1* and *gldt1* plants during CO₂ transition.

Plants were grown in high CO₂ (1500 ppm, HC) with a 10/14 h day/night cycle. After 8 weeks (growth stage 5.1, Boyes et al., 2001) plants were transferred in normal air (390 CO₂) with otherwise equal conditions. Leaf-material was harvested in HC (9 h light) and in normal air (1 and 9 h light), respectively. Shown are mean values \pm SD (n = 6) of selected metabolites quantified by LC-MS/MS analysis. For the full dataset including statistical evaluation please compare Supp. Table 1.

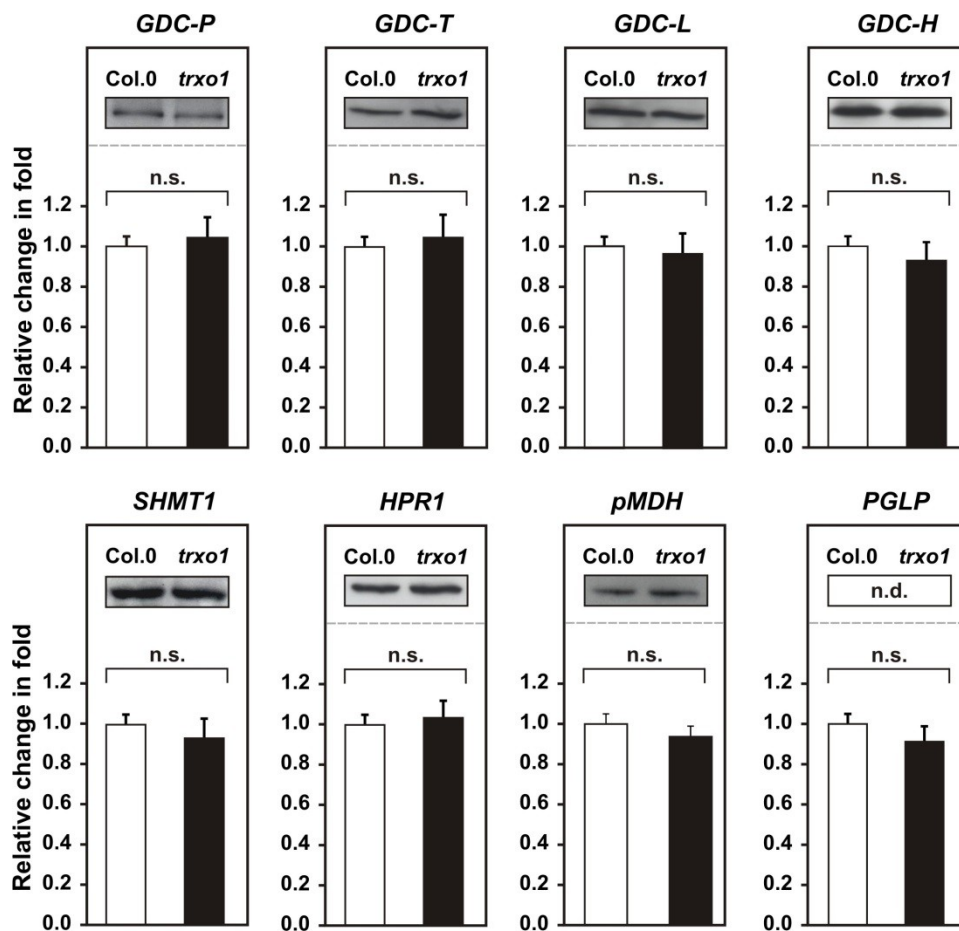


Figure 3. Expression of selected photorespiratory enzymes on the mRNA and protein level.

Plants were grown in normal air (390 ppm CO₂) with a 10/14 h day/night cycle. After 8 weeks (growth stage 5.1, Boyes et al., 2001), leaf-material was harvested at the end of the day (9 h illumination) and used for subsequent mRNA and protein extraction. Shown are mean values ± SD (n = 3) of mRNA expression determined by qRT-PCR analysis and representative immunoblots from the *trxo1* mutant compared to the control (n.s. – not significant; n.d. – not determined).

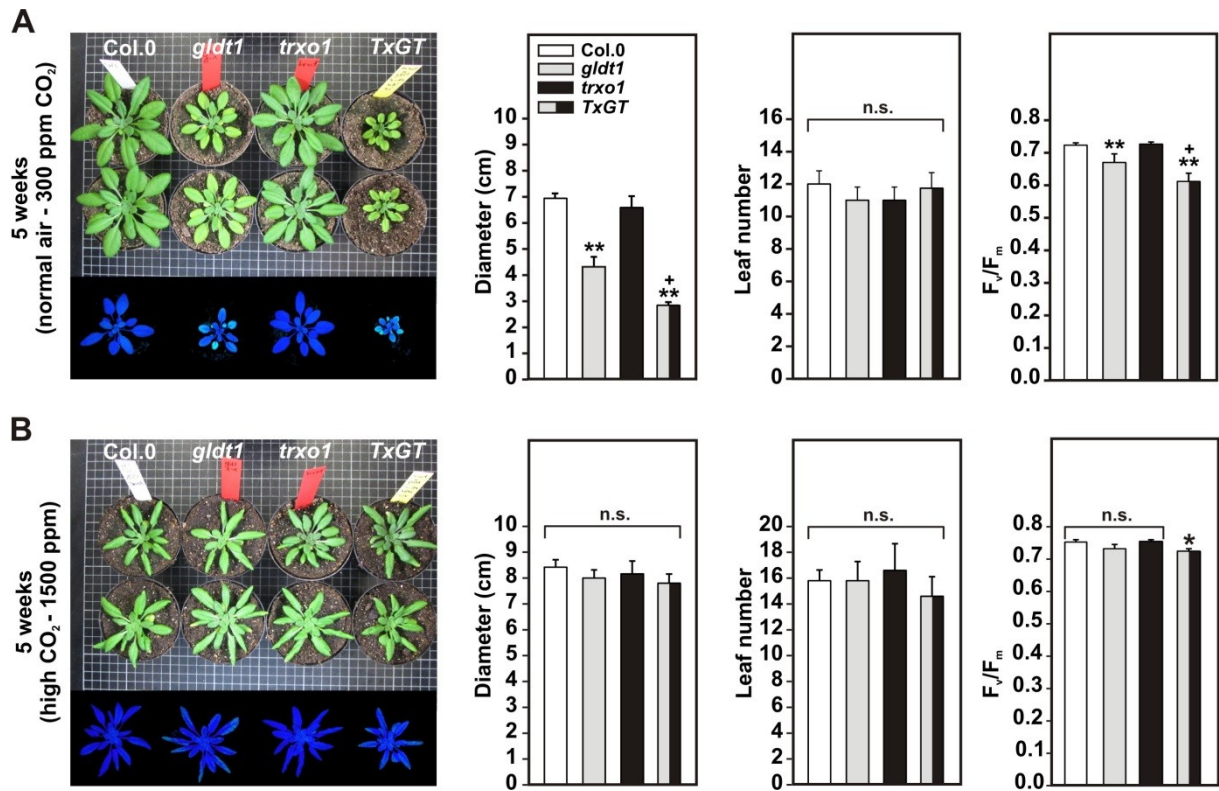


Figure 4. Phenotype, growth and chlorophyll a fluorescence of the *TxGT* double mutant.

Plants were grown in **(A)** normal air (390 ppm CO₂) or **(B)** high CO₂ (1500 ppm, HC) with a 10/14 h day/night cycle. After 5 weeks plants were photographed, rosette diameters and total leaf-numbers determined and chl_a fluorescence measurements carried out. Shown are mean values ± SD (n > 5). Asterisks indicate values significantly different from the control (*p < 0.05; **p < 0.01; n.s. – not significant) and plusses between the *gldt1* single and the *TxGT* double mutant (†p < 0.05).

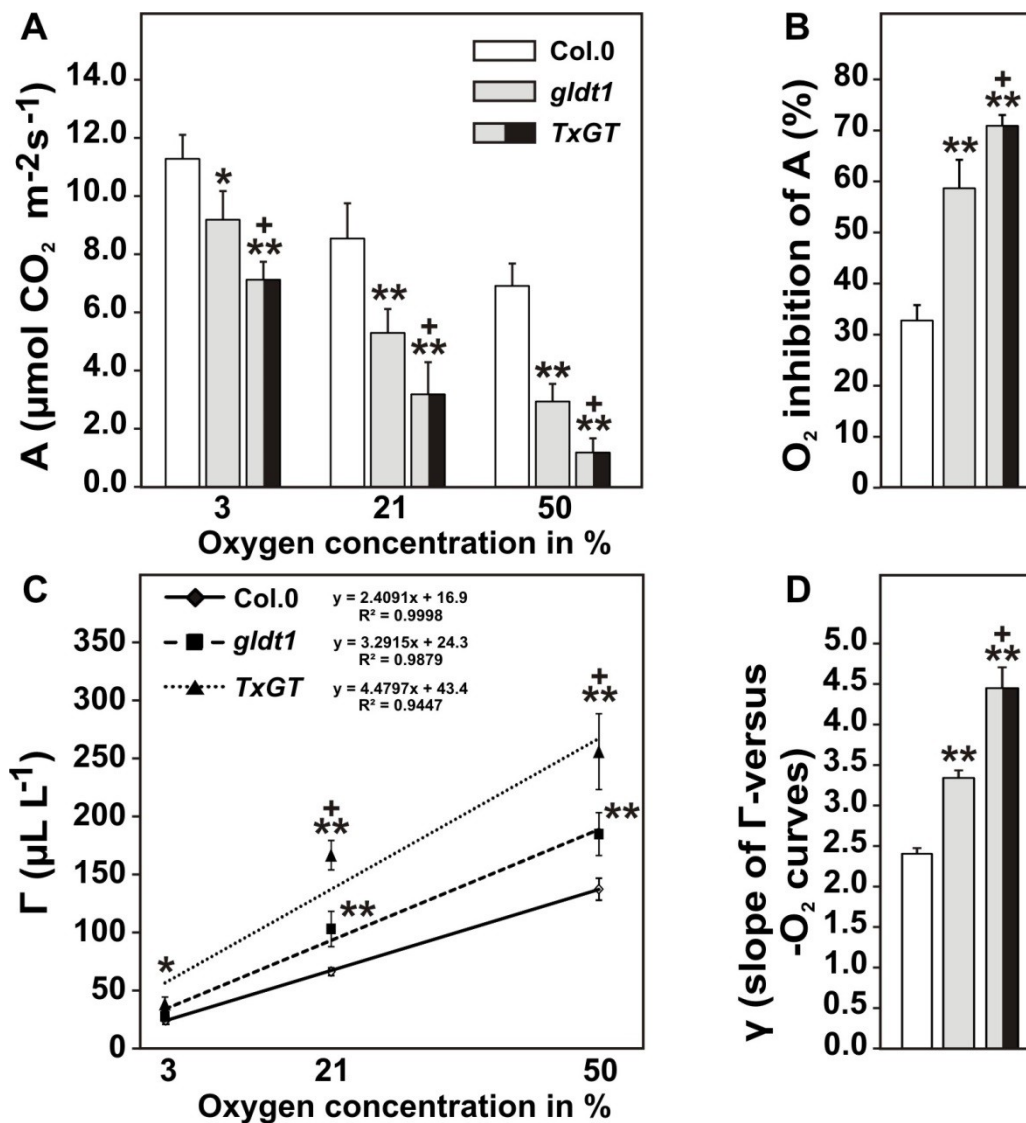


Figure 5. Oxygen-dependent gas exchange of *gldt1*, *TxGT* and the wild type.

Plants were grown in high CO₂ (1500 ppm) with a 10/14 h day/night cycle. After 7 weeks (growth stage 5.1, Boyes et al., 2001), plants were transferred to normal air (390 ppm CO₂) and used for gas exchange measurements at varying oxygen concentrations (3%, 21%, and 50%, balanced with N₂) after one week acclimation to the altered atmosphere. Mean values ± SD (n = 5-8) are shown for **(A)** net CO₂ uptake rates (A), **(B)** oxygen inhibition of A, **(C)** CO₂ compensation points (Γ) and **(D)** slopes of the Γ-versus-oxygen concentrations (γ). Asterisks indicate significant alterations of the mutants to the wild type according to Student's *t*-test (**p* < 0.05, ***p* < 0.01) and plusses between the *gldt1* single and the *TxGT* double mutant (+*p* < 0.05). For details on the calculation of oxygen inhibition and γ see material and methods section.

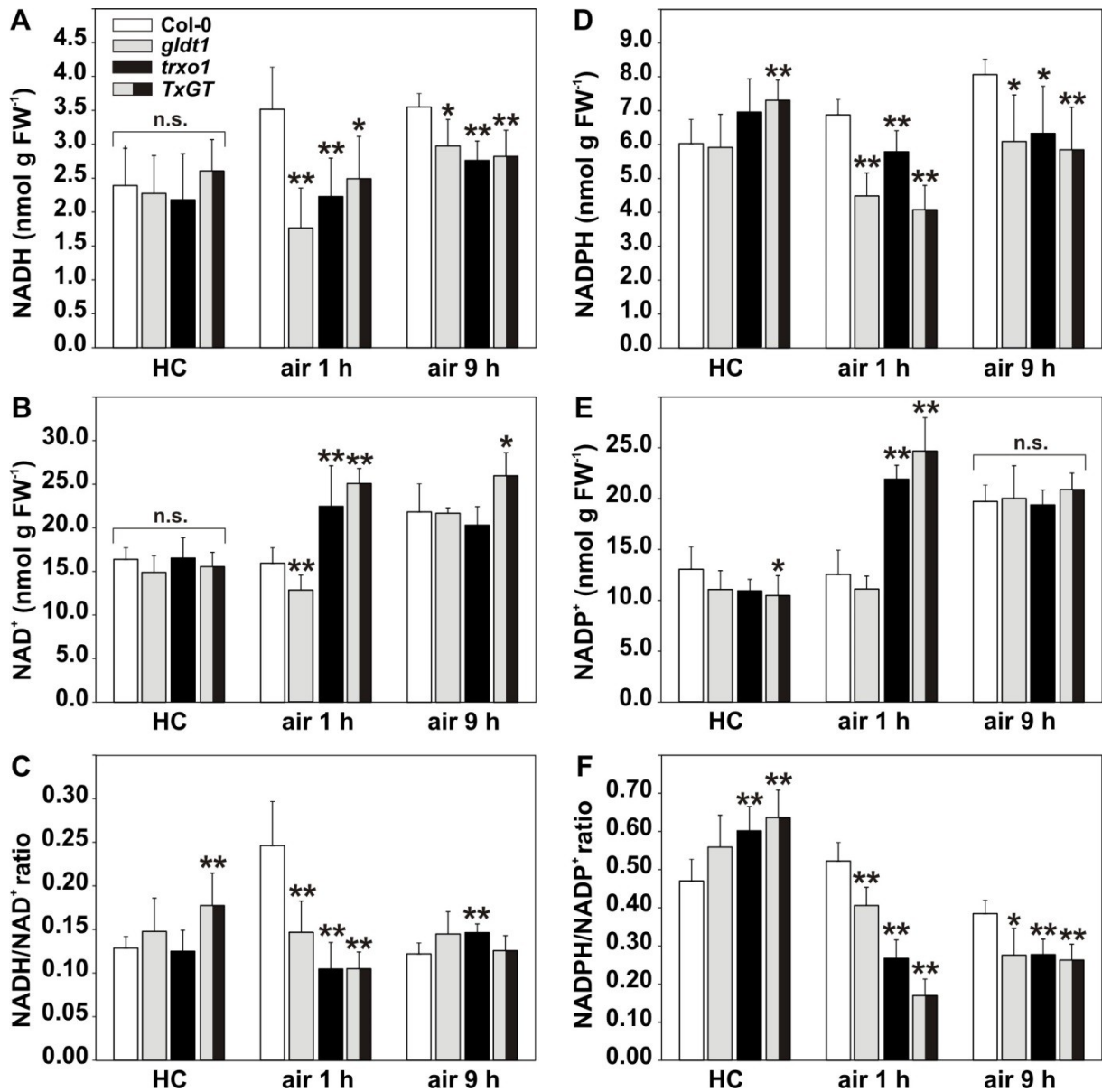


Figure 6. Pyridine nucleotide contents in wild type, *gldt1*, *trxo1* and *TxGT* plants during CO₂ transition.

Plants were grown in high CO₂ (1500 ppm, HC) with a 10/14 h day/night cycle. After 8 weeks (growth stage 5.1, Boyes et al., 2001) plants were transferred in normal air (390 ppm CO₂) with otherwise equal conditions. Leaf-material was harvested in HC (9 h light) and in normal air (1 and 9 h light), respectively. Shown are mean values ± SD (n > 6) of pyridine nucleotides (NAD⁺, NADH, NADP⁺ and NADPH) quantified by spectrophotometric analysis. Asterisks indicate significant alterations of the mutants to the wild type according to Student's *t*-test (*p < 0.05, **p < 0.01, n.s. – not significant).

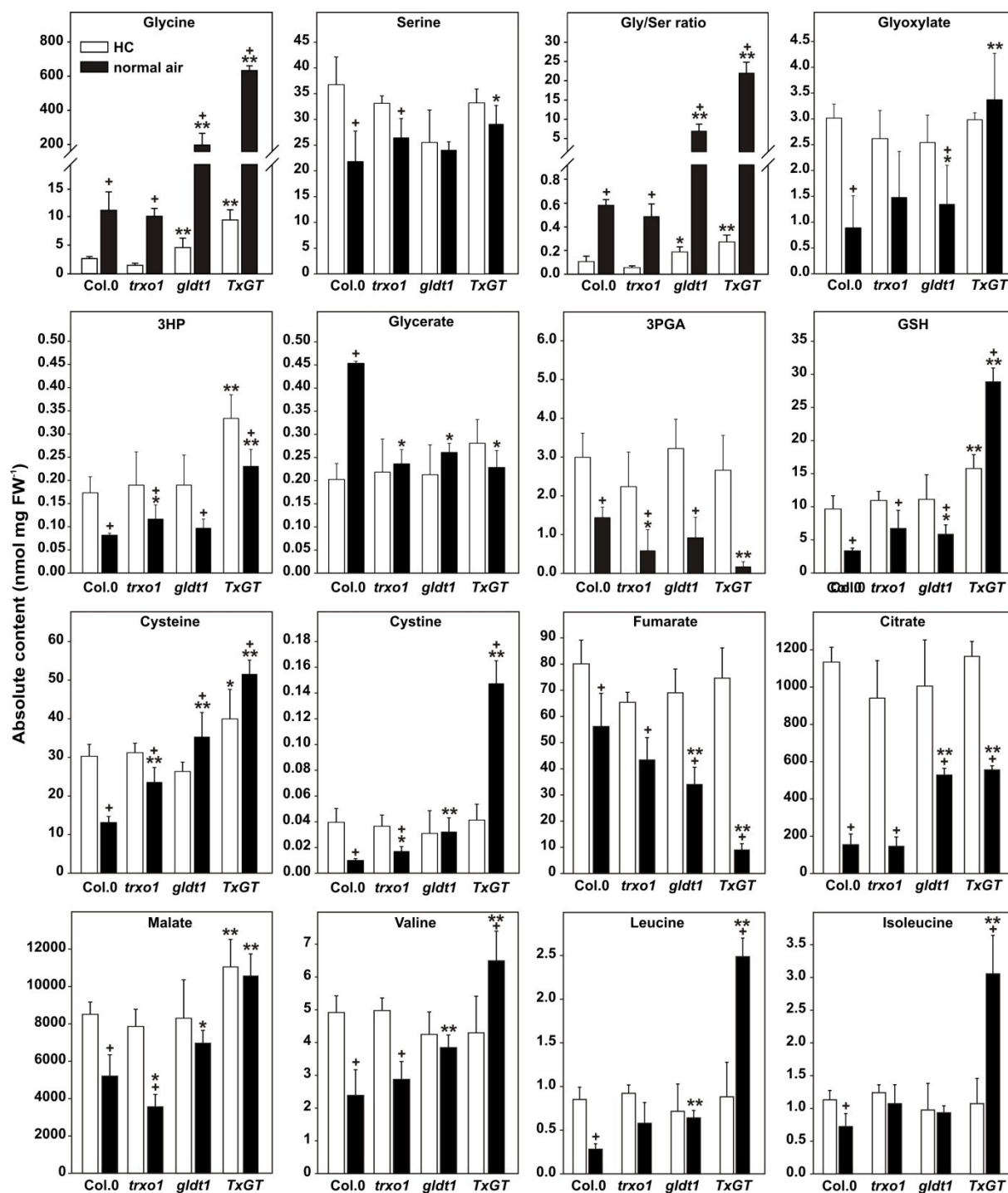


Figure 7. Levels of selected metabolites in leaves of the wild type, *trxo1*, *gldt1* and *TxGT* mutants grown in HC and normal air.

Plants were grown in high CO₂ (1500 ppm, HC) and normal air (390 ppm CO₂) with a 10/14 h day/night cycle. After 8 weeks (growth stage 5.1, Boyes et al., 2001), leaf-material was harvested in both conditions after 9 h illumination. Shown are mean values \pm SD ($n > 4$) of selected metabolites quantified by LC-MS/MS analysis. Asterisks indicate significant alterations of the mutants to the wild type in each condition according to Student's *t*-test

(*p<0.05; **p<0.01) and plusses between HC and normal air values of each genotype (*p<0.05). For a more comprehensive dataset including statistical evaluation please compare Supp. Table 2.

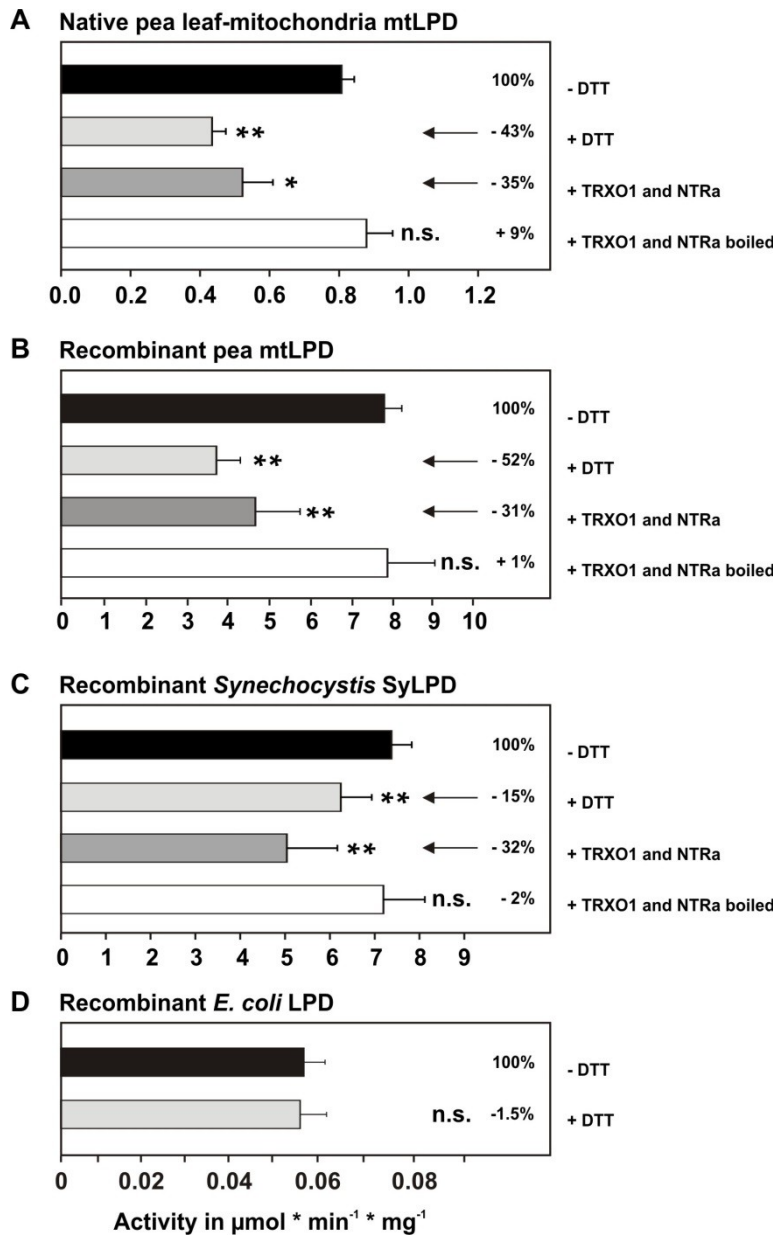


Figure 8. Redox-regulation of LPD from pea, *Synechocystis* and *E. coli*.

The activity of LPD proteins was determined in **(A)** pea leaf-mitochondria or of recombinant proteins produced through heterologous expression in *E.coli* and affinity purification from **(B)** pea, **(C)** *Synechocystis* and **(D)** *E.coli*, respectively. Shown are mean values \pm SD ($n > 4$) of LPD activity without or after addition of DTT and recombinant native or boiled TRXo1 and NTRa. Asterisks indicate significant alterations to the control according to Student's *t*-test (* $p < 0.05$, ** $p < 0.01$, n.s. – not significant). For experimental details see material and methods section.

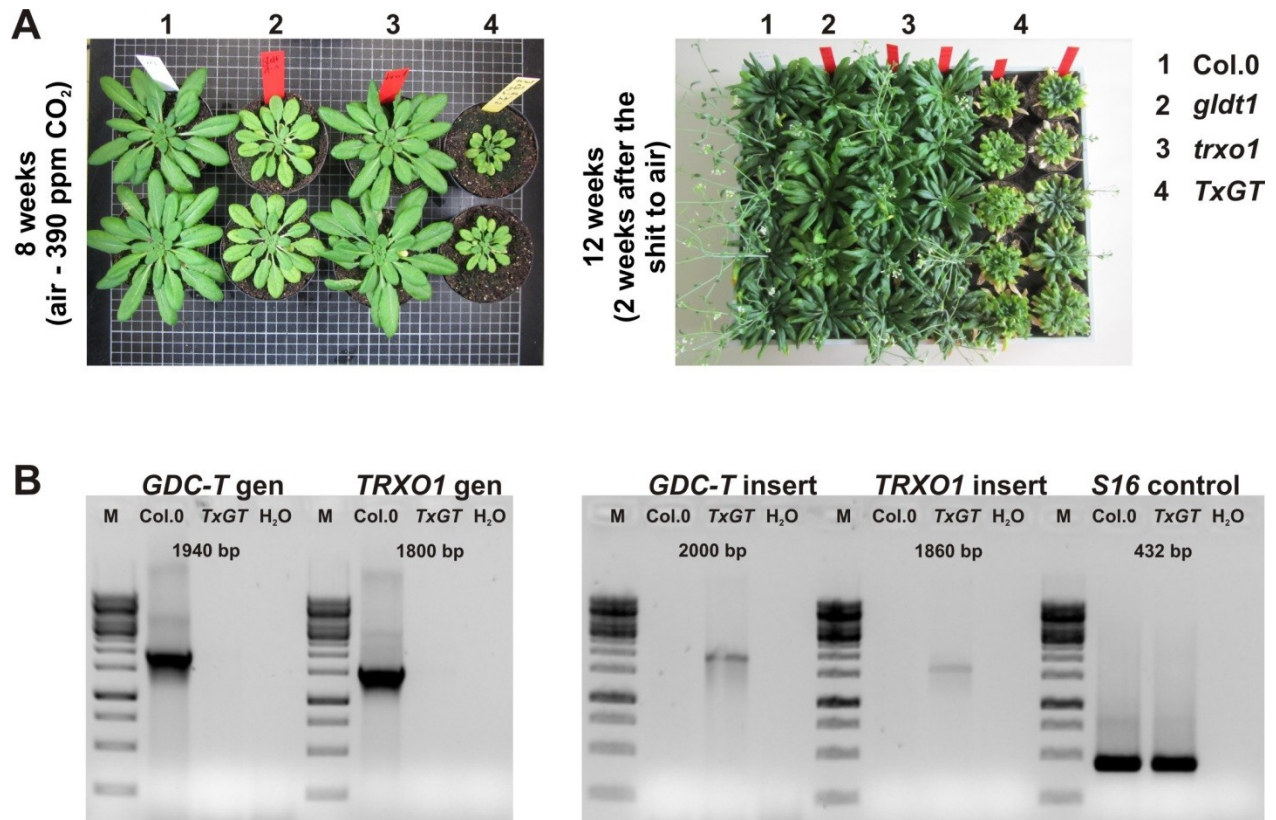
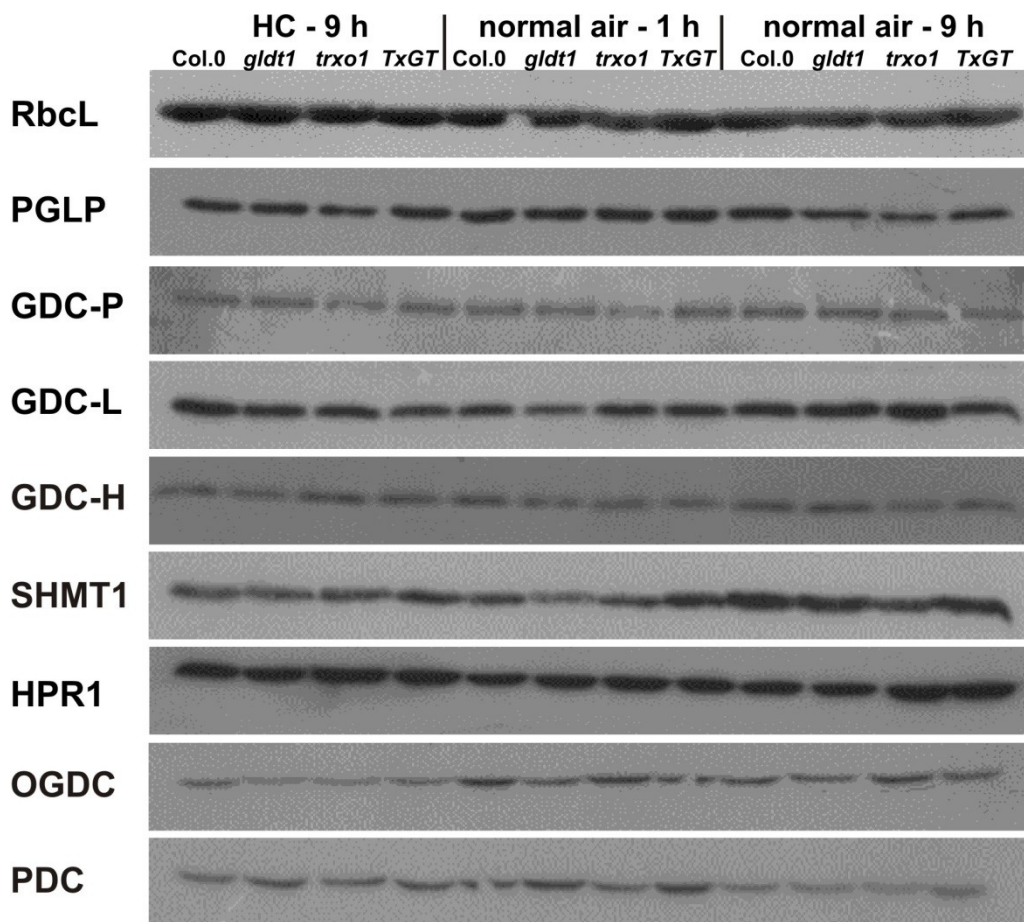


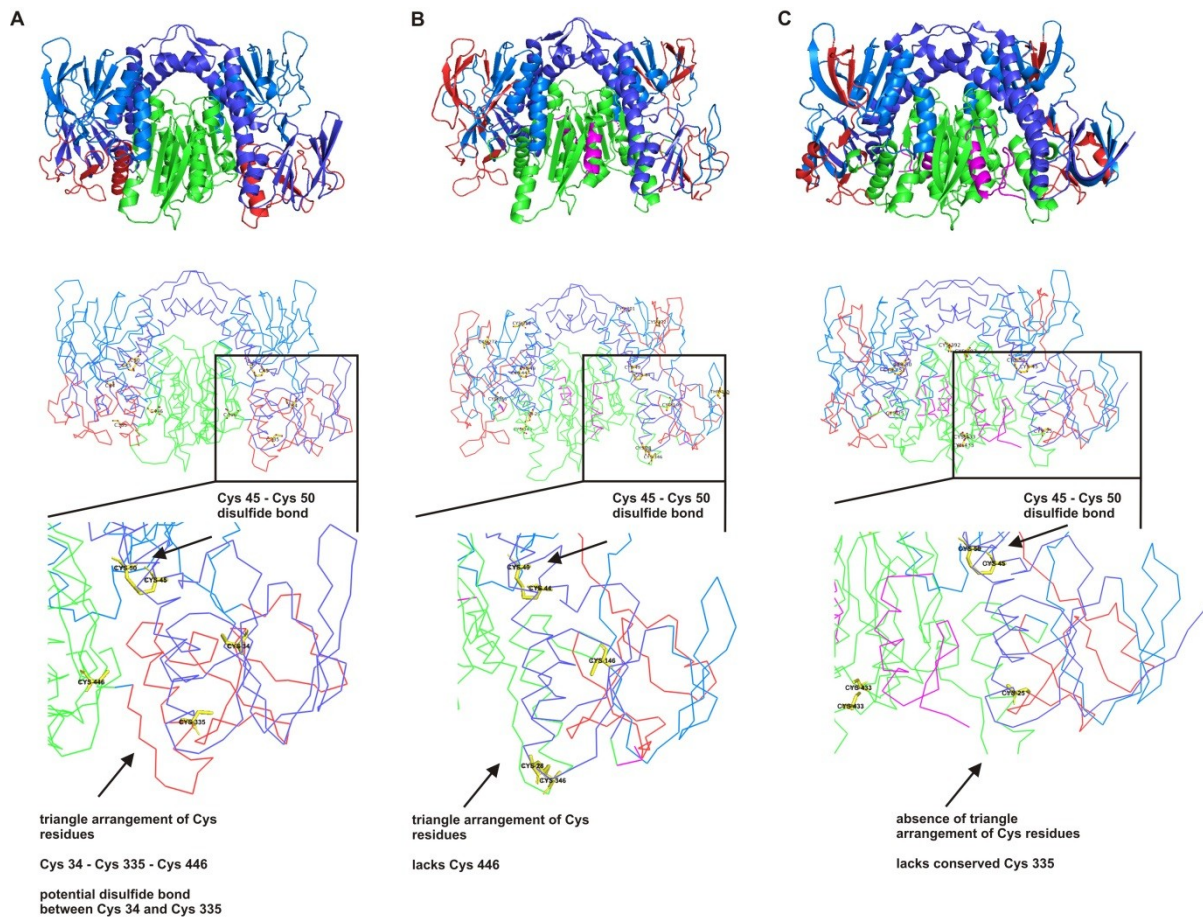
Figure 1. Phenotype and PCR verification of the *TxGT* mutant.

(A) Phenotype of the *TxGT* mutant compared to the *gldt1* and *trxo1* single mutants and the wild type after 8 weeks (left panel) in normal air (390 ppm CO₂) and after 12 weeks (right panel), 2 weeks after the transfer into normal air. **(B)** PCR verification of the *TxGT* mutant and the corresponding loading control (40S ribosomal protein *S16* gene). For primer combinations and PCR conditions please see material and methods section.



Supplemental Figure 2. Expression of selected photorespiratory and TCA cycle enzymes during CO₂ transition.

Plants were grown in high CO₂ (1500 ppm, HC) with a 10/14 h day/night cycle. After 8 weeks (growth stage 5.1, Boyes et al., 2001) plants were transferred in normal air (390 ppm CO₂) with otherwise equal conditions. Leaf-material (pools of 3 biological replicates) was harvested in HC (9 h light) and in normal air (1 and 9 h light), respectively, and used for subsequent protein extraction. Shown are mean representative immunoblots from the *gldt1*, *trxo1* and *TxGT* mutant compared to the wild type. Abbreviations: RbcL – Rubisco large subunit, PGLP – 2-phosphoglycolate phosphatase, GDC-P – glycine decarboxylase P-protein, GDC-L – glycine decarboxylase L-protein, GDC-H – glycine decarboxylase H-protein, SHMT1 – serine hydroxymethyltransferase 1, HPR1 – hydroxypyruvate reductase 1, OGDC – 2-oxoglutarate dehydrogenase complex E2 subunit, PDC – pyruvate dehydrogenase complex E2 subunit.



Supplemental Figure 4. 3D structures of selected LPD proteins.

Shown are LPD 3D structure models from **(A)** pea (P31023), **(B)** *Synechocystis* (P72740) and **(C)** *E.coli* (P0A9P0). The structures were produced in the program SWISS-MODEL using the resolved pea protein structure as template. Further processing to resolve CYS residues was carried out using PyMOL. Arrows indicate the predicted disulfide bond between the conserved Cys 45 and Cys 50 in all organisms and the triangle arranged Cys residues (Cys 34, Cys 335 and Cys 446) present only in sequences obtained from phototrophic organisms.